

Lawrence Berkeley National Laboratory

Recent Work

Title

THE PHOTOPRODUCTION OF NEGATIVE PIONS FROM DEUTERIUM

Permalink

<https://escholarship.org/uc/item/3zh5384h>

Author

Madey, Richard.

Publication Date

1952-01-09

UCRL-1634
UNCLASSIFIED

UNIVERSITY OF CALIFORNIA - BERKELEY

TWO-WEEK LOAN COPY

*This is a Library Circulating Copy
which may be borrowed for two weeks.
For a personal retention copy, call
Tech. Info. Division, Ext. 5545*

RADIATION LABORATORY

DISCLAIMER

This document was prepared as an account of work sponsored by the United States Government. While this document is believed to contain correct information, neither the United States Government nor any agency thereof, nor the Regents of the University of California, nor any of their employees, makes any warranty, express or implied, or assumes any legal responsibility for the accuracy, completeness, or usefulness of any information, apparatus, product, or process disclosed, or represents that its use would not infringe privately owned rights. Reference herein to any specific commercial product, process, or service by its trade name, trademark, manufacturer, or otherwise, does not necessarily constitute or imply its endorsement, recommendation, or favoring by the United States Government or any agency thereof, or the Regents of the University of California. The views and opinions of authors expressed herein do not necessarily state or reflect those of the United States Government or any agency thereof or the Regents of the University of California.

UNCLASSIFIED

UNIVERSITY OF CALIFORNIA

Radiation Laboratory

Contract No. W-7405-eng-48

THE PHOTOPRODUCTION OF NEGATIVE PIONS FROM DEUTERIUM

Richard Madey

(Thesis)

January 9, 1952

Berkeley, California

THE TABLE OF CONTENTS

	Page
I. THE ABSTRACT	6
II. THE INTRODUCTION	9
A. The Production of Pions by Photons	9
B. The Negative to Positive Ratio of the Photo-Pion Production Cross Sections	9
1. Deuterium	9
2. Other Light Nuclei except Beryllium and Calcium	10
3. Beryllium	11
4. Calcium	12
C. The Photo-Production of Positive Pions	12
D. The Photo-Production of Neutral Pions	13
E. The Present Status of Photo-Pion Production	13
III. THE THEORY OF PION-PROTON COINCIDENCES PHOTO-PRODUCED FROM A NEUTRON	15
A. The Angular Correlations	15
1. The Target Neutron is Unbound or "Free" and at Rest	15
2. The Target Neutron is Unbound or "Free" and has a Momentum Distribution	18
B. The Energy Correlations	23
IV. THE EXPERIMENTAL METHOD	25
A. The Photon Source	25
1. The Duty Cycle of the Beam Pulse	25
2. The Energy Distribution of the Photons	27

	Page
IV. A. 3. The Collimation	30
a. The Primary Collimation	30
b. The Secondary Collimation, and the Shielding of the Counters	31
4. The Integration of the Beam Intensity	33
5. The Alignment of the Experimental Apparatus with the Direction of the Photon Beam	33
B. The Target	34
1. The Choice of Heavy Water; Subtraction of Back- ground by Using Ordinary Water	34
2. The Thickness	35
3. The Orientation	37
4. The Containers	38
5. The Reduction of Systematic Errors	39
C. The Scintillation Counter Telescopes	39
1. The Two Experimental Arrangements	39
2. The Telescope Geometries; Areas, Designations, Thicknesses, Spacings, and Mountings of the Phosphors	41
a. Areas of the Phosphors	41
b. Designations of the Phosphors	41
c. Thicknesses of the Phosphors	41
d. Spacings between the Phosphors	42
e. Mountings of the Phosphors	42
3. The Proton and the Pion Detection Thresholds	43
D. The Absorbers	43
1. The Choice of Materials	43
2. The Selection of Thicknesses	44

	Page
IV. E. The Angular Resolution	45
1. The Effect of the Finite Size of the Target and of the Detectors	45
2. The Effect of Multiple Scattering in the Target	47
F. The Electronic Instrumentation	48
1. A Descriptive Survey	48
a. Introduction	48
b. The Block Diagrams of the Two Experimental Arrangements	48
c. The Photomultiplier and Limiter Circuit	48
d. The Coincidence Circuits	49
e. The Phase Inverting Distributed Amplifiers	49
f. The Overall Performance of the Counting System	50
2. The Shaping of the Scintillation Counter Pulses	50
a. The Pulse Shaping Problem	50
b. The Two Limiter Solution to the Pulse Shaping Problem	50
(1) The Functions of the Limiters	50
(2) The Design Considerations	51
V. THE RESULTS	53
A. The Angular Correlations	53
B. The Energy Correlations	54
C. The Time Correlations	56
D. The Co-Planarity	57
E. The Yield	57
F. The Net Charge of the Reaction Products	58
G. The Total Angular Momentum of the Reaction Products	58

	Page
VI. SOME EXTENSIONS OF THE EXPERIMENT	59
A. The Excitation Function and the Production Cross-Sections	59
B. The Spin-Flip Probability	59
C. Pion-Proton Coincidences from Beryllium	61
D. The Artificial Production of the V^0 Particle	61
E. Momentum Distributions in Nuclei	61
F. Development of a Detector of Negative Pion "Stars"	62
VII. THE ACKNOWLEDGEMENTS	63
VIII. THE REFERENCES	64
IX. THE ILLUSTRATIONS	67

THE PHOTOPRODUCTION OF NEGATIVE PIONS FROM DEUTERIUM

Richard Madey

Radiation Laboratory, Department of Physics
University of California, Berkeley, California

January 9, 1952

I. THE ABSTRACT

Evidence is presented for the observation of the photo-pion production process $\gamma + n \rightarrow \pi^- + p$. The source of photons is the 322 Mev bremsstrahlung from the Berkeley synchrotron. The target neutrons are the very loosely bound neutrons in deuterium nuclei. The method of identification of negative pions consists of studying the angular correlation of pion-proton coincidences.

The energy and momentum conservation laws for the photo-pion production from a free neutron at rest predict correlated pairs of pion and proton angles that are very nearly independent of photon energy in the photon energy interval from about 200 Mev to about 1000 Mev, and for laboratory pion angles from about 60° to 180° . For example, for a laboratory pion angle of 90° , the proton angle changes from 30.5° at a photon energy of 200 Mev to a maximum of about 32.5° at a photon energy of about 320 Mev and then gradually decreases to 25.1° at a photon energy of 1000 Mev; thus, the total variation in proton angle is about 7.5° for photon energies from 200 Mev to 1000 Mev. The loose binding of the neutron in deuterium imparts a calculable smearing of the angular correlation. Further, the upper energy limit of 322 Mev of the bremsstrahlung

spectrum from the Berkeley synchrotron restricts the protons to come off in the forward direction within an angular region of about sixty degrees from the beam direction.

The experimental evidence for the reaction $\gamma + n \rightarrow \pi^- + p$ may be summarized as follows:

1. The difference in the counting rates from heavy water and ordinary water targets has a well-defined peak. This peak occurs at those pairs of correlation angles that are predicted for the photo-production of a negative pion from a free neutron at rest. When the angle of the proton detector is varied on either side of the predicted correlation angle, by an amount equal to the angular resolution of the proton detector, the heavy water-ordinary water difference counting rate essentially disappears.

2. The difference in the counting rates from heavy water and ordinary water targets essentially disappears when absorbers, which are calculated to stop the maximum expected energy of either a pion or a proton, are inserted in either the pion or the proton detector.

3. At least two ionizing particles are detected in time coincidence. The simultaneity of detection is ascertained within the resolution time of 2×10^{-8} seconds.

4. Within experimental error, the process is co-planar. The heavy water-ordinary water difference counting rate essentially disappears when the pion detector is tilted out of the plane containing the photon beam and the proton detector.

5. The yield of the heavy water-ordinary water difference counting rate at the correlation angles is compatible with a photo-pion production cross section.

6. The net charge of the reaction products is zero.

7. The total angular momentum of the reaction products is half-odd integral.

Some extensions of this experiment are discussed briefly.

THE PHOTOPRODUCTION OF NEGATIVE PIONS FROM DEUTERIUM

Richard Madey

Radiation Laboratory, Department of Physics
University of California, Berkeley, California

January 9, 1952

II. THE INTRODUCTION

A. The Production of Pions by Photons

The experimental investigations of the nature of the pion field and of the character of the pion-nucleon coupling was limited to cosmic ray studies prior to the laboratory discovery (1948), by Lattes and Gardner,¹ of the artificial production of pions by bombardment of targets with high energy nucleons from the Berkeley cyclotron. No direct cosmic ray experiments have been performed with photon produced pions; however, the production of pions by photons, which were generated by the Berkeley synchrotron, was definitely established in 1949 by McMillan and Peterson.²

B. The Negative to Positive Ratio of the Photo-Pion Production Cross Sections

1. Deuterium

The experimental evidence is fairly good that the negative to positive photo-pion production ratio from deuterium has a value close to unity and is relatively insensitive either to the energy or to the angle of production.^{3,4} If the neutron and the proton in the deuteron act as free particles, except for the small binding energy and except for the exclusion principle effects, then this experimental result is an argument

that the nucleonic charge should not affect the photo-pion production process except for determining the pionic charge.

Theoretical calculations have been made by Breuckner⁵ of the negative to positive ratio for the photo production of pions from free nucleons. If the interaction of the electromagnetic field of the photon is assumed to be only with the currents resulting from the charges of the moving protons and pions, then the calculation yields a ratio of the negative to the positive cross sections that depends both on the energy and the angle of pion production and that has values always greater than one; on the other hand, if the photon interaction with the magnetic moment of the struck nucleon is the predominating interaction, then the resulting theoretical expression for the negative to positive ratio is essentially independent both of the energy and the angle of production and is nearly unity, if the numerical values of the anomalous magnetic moments, which are observed in a static field, are used. Thus, the theory of the production process is in agreement with the experimental results if the predominant interaction of the photon is with the magnetic moment rather than with the moving charges of the struck nucleons.

2. Other Light Nuclei except Beryllium and Calcium

Several investigators^{4,6,7,8,9} have contributed to our present knowledge of the negative to positive photo-pion production ratio from light nuclei. For each of the light nuclei, except beryllium and calcium, the minus to plus ratio has a value near unity. Furthermore, the minus to

plus ratio from carbon was found by McMillan, Peterson and White,⁶ and by Peterson, Gilbert and White⁷ to be fairly independent of both the energy and the angle of observation. The effect of nuclear structure on this ratio is not easily interpretable quantitatively, because the pion-nucleon interaction may be different for the photo-production from a bound nucleon than from a free nucleon, and also because the nuclear interactions of the pions before leaving the nucleus have to be considered. If these two considerations are neglected for the photo-pion production from carbon, then the interpretation is the same as that for deuterium, namely that the predominant interaction of the photon is with the magnetic moment rather than with the moving charges of the struck nucleons.

3. Beryllium

Littauer and Walker⁴ used a double focusing magnetic analyzer of Camac¹⁰ to focus charged pions onto an array of counters, and compared the positive to negative ratios from carbon and beryllium for pions which were produced by photons at a pion production energy of about 50 Mev and at a pion production angle of 135° . Their result from carbon was 1.04 ± 0.05 ; from beryllium, 2.25 ± 0.11 . Medicus¹¹ applied the nuclear emulsion detection method at Berkeley to obtain a negative to positive production ratio from beryllium of 2.0 ± 0.3 in the energy range from 40 to 70 Mev and at an angle of 90° to the beam direction. The magnitude of the difference between the carbon and the beryllium ratios can not be

explained merely by the higher neutron-proton ratio in the beryllium nucleus, but rather indicates that the very loose binding of the extra neutron in beryllium allows it to participate more actively in the production process than the other more tightly bound nucleons.

4. Calcium

An especially prominent deviation from a negative to positive ratio near unity was found by Littauer and Walker⁴ in the "doubly magic" Ca^{40} nucleus. The relatively low value of 0.58 ± 0.06 is attributed to the shell structure of the Ca nucleus.

C. The Photo-Production of Positive Pions

Cook¹² used nuclear emulsions to detect the photo-production of pions from a liquid hydrogen target. Steinberger and Bishop developed and used an electronic method of positive pion detection to study the photo-production of positive pions from hydrogen.¹³ The results of later work¹⁴ produced an excitation function, an angular distribution from 250 Mev photons, and an energy distribution at 90° to the photon beam direction. Mozley¹⁵ employed this same electronic method of positive pion detection to measure the dependence on the atomic number of the production cross section at the production energies of 42 Mev and 76 Mev and at the production angle of 90° .

The excitation curve rises steeply for low photon energies and then appears to level off at a photon energy of about 250 Mev. The angular distribution, in the center of mass coordinates, is fairly isotropic but perhaps with a slight peak in the backward direction. The number of

positive pions produced per nucleon in the target may be approximately fitted by an $A^{-1/3}$ curve, where A is the mass number of the target nucleus. Littauer and Walker⁴ arrived at the same conclusion for the dependence on the mass number A , but obtained a better fit if the sum of positive and negative pions is plotted as a function of A .

D. The Photo-Production of Neutral Pions

Panofsky, Steinberger, and Steller¹⁶ have used the gamma-gamma coincidence technique to study the photo-production of neutral pions. The angular distribution of the neutral pions from beryllium was found to be strongly peaked in the forward direction in the laboratory. The dependence on the mass number A of the production obeys an $A^{2/3}$ law. Their present data for production in hydrogen show that the neutral and positive pion production cross sections are comparable and that the neutral pion excitation curve starts more slowly from threshold than the positive pion photo excitation curve. These conclusions for neutral pion production by photons on hydrogen have been verified independently by the experiment of Silverman and Stearns¹⁷ at Cornell.

E. The Present Status of Photo-Pion Production

Pion production by photons on free nucleons is one of the simplest pion processes; yet the available information about positive and neutral pions produced by photons on free protons^{13,14,16,17} has not been interpreted satisfactorily by current pion theories. Recently, phenomenological or semi-phenomenological theories^{18, 19, 20, 21, 22} have been advanced,

for the treatment of photo-pion reactions in light nuclei, because the phenomenological method is expected to be applicable, independent of what pion theory and what pion-nucleon coupling finally turns out to be correct. Photo-production experiments from isotopes with a large number of nucleons may yield information about nuclear structure and about the pion interaction with the nucleons of the nucleus in which the pion is produced. Further experimental information concerning the initial act of production of the pion itself may be obtained by studying negative pion production by photons on free neutrons.

Negative pion production data have not kept pace with positive and neutral pion production data chiefly because electronic or other counting techniques for facilitating the study of negative pion production have not kept pace with the electronic methods of positive and neutral pion detection.

The present paper describes a method for employing scintillation counters to investigate the photo-production of negative pions from essentially free neutrons.

III. THE THEORY OF PION-PROTON COINCIDENCES PHOTO-PRODUCED FROM A NEUTRON

A. The Angular Correlations

1. The Target Neutron is Unbound or "Free" and at Rest

The method of identification of negative pions simply consists of studying the angular correlation of pion-proton coincidences. The angular correlation for this process is predicted from the energy-momentum conservation laws. In fact, on close examination, the conservation laws for this particular two-body process, where the target neutron in the deuteron is considered to be an unbound or "free" neutron at rest in the laboratory, yield several very useful and very interesting results.

Probably the most interesting result is the one which states that the resultant pairs of correlated pion and proton angles are very nearly independent of photon energy over a wide range of both photon energies and pion angles. A plot (Figure 1) of pion angle θ versus proton angle χ , for various values of photon energy k , reveals the fact that the correlated pion and proton angles are very nearly independent of photon energy for laboratory photon energies from about 200 Mev to about 1000 Mev and for laboratory pion angles from about 60 degrees to 180 degrees.

This first result is not a very obvious result because the expected solution of the conservation laws for this process contains a photon energy dependence; that is, the expected solution in the laboratory coordinate system would have the functional form

$$F(\theta, \chi, k) = 0, \quad (1)$$

where θ and χ are the angles, measured with respect to the direction of the photon beam, of pion and proton emission, respectively, and k is the photon energy. Now, this functional relationship may be represented by a surface. Each point on the surface is specified by a set of values for θ , χ , and k . A cross sectional view of this surface for a pion angle θ of 90° (Figure 2) illustrates the exact dependence of the proton angle χ on the photon energy k .

The physical interpretation of the independence of the angular correlation in the plane on the photon energy is the following. As the photon energy increases, both the energy available for the collision in the center of mass coordinate system and the velocity of the center of mass increase; however, as a consequence of the particular masses that are involved in the final state of the photo-pion production process, the increases in the center of mass velocity and in the available energy are such that, for a given production angle in the center of mass coordinate system, nearly constant values are preserved for the ratios of both (a) the center of mass velocity to the velocity of either particle in the center of mass coordinate system, and (b) the momentum of the center of mass to the momentum of either particle in the center of mass coordinate system.

The photon energy region, which is of interest in demonstrating the angular correlation in this particular experiment, is about 100 Mev wide, extending from about 220 Mev to 320 Mev. The upper energy limit of the bremsstrahlung spectrum of the Berkeley synchrotron determines

the 320 Mev limit; the energy threshold of the proton detection apparatus used in the experiment imposes a lower limit on the photon energy in the neighborhood of 220 Mev.

The limits on the angular position of the pion telescope are set essentially by the restrictions on the correlated angular positions of the proton telescope. The limits on the proton angles are determined by the experimental apparatus and by the geometry used in this particular experiment. The proton telescope cannot be moved to angles smaller than about 10° from the beam direction without introducing too many accidental coincidences. The upper limit on the laboratory proton angle is set both by the energy threshold of the proton detector and by the degradation of proton kinetic energy by absorption in the target. A practical upper limit on the proton angle turns out, as will be shown later, to be about 30° . This spread of about 20° in the allowable proton angle corresponds to an allowable spread of about 60° , from about 90° to about 150° , in the correlated pion angles.

Figure 1 shows the degree of angular correlation over the complete range of proton and pion angles and photon energies; on the other hand, Figure 3 shows the degree of angular correlation only over that range of proton and pion angles and photon energies which are experimentally observable in this experiment. The laboratory angular resolution for both telescopes is also indicated in Figure 3 for comparison with the degree of angular correlation. The total change in proton angle over the photon energy interval from 220 Mev to 300 Mev

is seen to be (a) less than 3.5° for a pion angle of 90° , and (b) about 1.5° for a pion angle of 135° .

Probably the most useful result is the one which states that the energy limit, k_{\max} , of the bremsstrahlung spectrum restricts the protons to come off in the forward direction within an angular region of about sixty degrees (for $k_{\max}=322$ Mev) measured from the beam direction. Figure 4 is a calculated curve of the maximum allowable proton angle as a function of photon energy.

It is a very simple matter to apply this second result to the design of this experiment. The pion angle is simply chosen to be greater than the maximum proton angle allowed by the upper energy limit of the bremsstrahlung spectrum. Figure 5 is a vector momentum diagram, which illustrates this choice in pion angle.

The usefulness of this second result arises from the fact that the restriction against protons being emitted along the direction of the pion momentum vector simplifies the study of the negative pions themselves.

All of the above results depend, through the conservation laws, only on the total energy of the system, the total momentum of the system, and the masses of the particles in the final state of the photo-pion production process.

2. The Target Neutron is Unbound or "Free" and has a Momentum Distribution

In actuality, the target neutrons are not free neutrons at rest in the laboratory, but are the very loosely bound neutrons in

deuterium nuclei. It must be ascertained that the angular correlation that is predicted for a free neutron at rest is not fuzzed out too much by the momentum distribution of the target neutrons in deuterium nuclei. The relatively small value of the 2.2 Mev binding energy of the neutron in the deuteron has a negligible effect on the energy conservation equation for this process; however, a momentum of the order of magnitude of the average momentum of the target neutron in the deuteron cannot be neglected in the momentum conservation equations. An estimate of the degree of fuzziness that is introduced into the angular correlation has been obtained by treating the neutron in the deuteron as an unbound or "free" neutron with a momentum distribution which is appropriate to that of a neutron bound in the deuteron.

The solution of the conservation laws for the photo-pion production process from a target neutron that has a vector momentum \vec{P}_n , may be expressed in the functional form

$$G(\theta, X, k, \vec{P}_n) = 0, \quad (2)$$

where the variables θ , X , and k have the same meaning as in the case of the free neutron at rest. The vector \vec{P}_n is completely specified by three spherical polar coordinates.

Ideally, the detectable pion-proton coincidences are confined to a plane that is defined by the geometry of the experimental arrangement. Actually, the detectable pion-proton coincidences are confined to a set of planes that are contained within an azimuthal range defined by the

finite size of the photon beam, the target, and the detectors. Since most of the target neutrons in deuterium are contained within a momentum sphere of radius equal to about 45 Mev, the majority of these neutrons can contribute pion-proton pairs into the azimuthal range allowed by the detectors. Thus, the order of magnitude of the smearing of the angular correlation in a plane is estimated more simply by dealing with the projection onto this plane of the vector momentum of the target neutron rather than with the vector momentum itself. The projected momentum vector is completely specified by the two plane polar coordinates P_n and ψ , where now P_n is the magnitude of the projection onto the plane of the laboratory momentum vector of the target neutron, and ψ is the laboratory angle, measured with respect to the direction of the incident photon momentum, of the projected vector momentum of the target neutron. The smearing of the angular correlation in the plane was calculated for representative values of the variables P_n , ψ , and k . Typical results are illustrated in Figures 6 and 7.

The vector momentum diagram (Figure 8), in the laboratory coordinate system, for the photo-pion production from a free neutron with a vector momentum can be used to facilitate the qualitative discussion of the effects of the vector momentum of the target neutron in the deuteron, on the angular correlation in the plane. For fixed values of both the photon energy k and the magnitude of the projected momentum P_n , two different effects cause the smearing of the planar angular correlation. One

effect arises from changes in the magnitude of the velocity of the center of mass with the associated changes in the energy that is available in the center of mass coordinate system; the other, from changes in the direction of the velocity of the center of mass.

The magnitude effect can be illustrated by considering the collision for $\psi = 0^\circ$. Then, the velocity of the center of mass is greater and therefore the energy available for the collision in the center of mass coordinates is smaller than for the case of the free neutron at rest where $P_n = 0$; however, for a given production angle in the center of mass coordinate system, the increased center of mass velocity and the decreased particle velocities in the center of mass coordinate system both cause the pion and the proton to be thrown farther forward, in the direction of decreasing angles θ and X , in the laboratory coordinate system than for the case of the free neutron at rest. Similarly, consideration of the collision for $\psi = 180^\circ$ leads to the opposite conclusion that both the pion and the proton are thrown farther backward, in the direction of increasing angles θ and X , in the laboratory coordinate system than for the case of the free neutron at rest.

The direction effect can be illustrated by considering the collision for ψ equal to either 90° or 270° . The magnitude effect is very small here because the magnitude of the velocity of the center of mass changes very little for these values of ψ as long as P_n^2 is small compared to k^2 ; however, the direction of the velocity of the center of mass is change by an angle δ , measured with respect to the photon beam direction,

where (see Figure 8)

$$\sin \delta = \frac{P_n}{P_T} \sin \psi \quad (3)$$

or

$$\tan \delta = \frac{P_n \sin \psi}{k + P_n \cos \psi} \quad (4)$$

The transformation of the correlation angles from the center of mass coordinate system to the laboratory coordinate system gives pairs of correlated pion and proton angles, θ_β and X_β , that are measured with respect to the direction of the velocity of the center of mass for the collision. The pairs of correlated pion and proton angles, θ and X , that are measured with respect to the direction of the photon beam, are obtained from the angles θ_β and X_β by properly applying the correction angle δ . The correction angle δ increases one of the angles and decreases the other. For the collision in the plane at $\psi = 90^\circ$,

$$X = X_\beta + \delta \quad (5)$$

and

$$\theta = \theta_\beta - \delta \quad (6)$$

whereas, for the collision in the plane at $\psi = 270^\circ$,

$$X = X_\beta - \delta \quad (7)$$

and

$$\theta = \theta_\beta + \delta \quad (8)$$

Thus, for the collision at $\psi = 90^\circ$, the direction effect causes (a) the proton to be thrown farther backward, in the direction of increasing angle X , and (b) the pion to be thrown farther forward, in the direction of decreasing angles θ , in the laboratory coordinate system, than for the

comparison case of the free neutron at rest where $P_n = 0$. The opposite conclusions are true for the collision at $\psi = 270^\circ$.

Figures 6 and 7 indicate the tendency to form double-lobed distributions for the emission probability at a proton angle χ , for a fixed pion angle θ and a fixed photon energy k , when a fixed value of the projected neutron momentum P_n is considered at various polar angles ψ . The values of ψ from 90° to 180° , and from 270° to 360° , form the two lobes; the transition from one lobe to the other occur for values of ψ between 0° and 90° and between 180° and 270° . The displacement of the curves at $\psi = 0^\circ$ and 180° is caused by the variation in the magnitude of the velocity of the center of mass, the displacement of the curves at $\psi = 90^\circ$ and 270° is caused by the variation in the direction of the velocity of the center of mass.

B. The Energy Correlations

For a given pair of pion and proton correlation angles, a definite interval of pion kinetic energies is correlated with each interval of photon kinetic energies. By specifying the proton angle and the photon energy, both the proton kinetic energy and the pion kinetic energy are uniquely determined. Thus, if such points on the proton kinetic energy-pion kinetic energy plane are connected both by lines of constant proton angle and by lines of constant photon energy, the result is the grid-like network of Figure 9. Figure 9 both illustrates the energy correlations and provides a handy though approximate guide for selecting absorbers so that the production from certain photon energy intervals can be studied.

For simplicity, the above discussion has concerned the free neutron at rest. The modifications that result from the momentum distribution of the deuteron neutrons have been calculated for use in the experiment.

IV. THE EXPERIMENTAL METHOD

A. The Photon Source

1. The Duty Cycle of the Beam Pulse

The Berkeley synchrotron accelerates electrons to a maximum energy of $322 \pm 6 \text{ Mev}$ ²³ at the target radius* and in a magnetic field which rises sinusoidally to its peak value of 11,400 gauss in about 7900 microseconds.²⁴ The pulse repetition rate is six per second.

Since the radius of the equilibrium electron orbit is fixed at the nominal design value of one meter, the synchrotron design equations show that the electron beam energy is a function only of the magnetic field at the equilibrium orbit. If the electrons lost no energy, by radiation for example, then the minimum amplitude or envelope of the radio frequency accelerating voltage, which is required to barely sustain the electrons in the equilibrium orbit, is proportional to the rate of change of the magnetic field. Since the time variation of the magnetic field is an increasing sinusoid during the electron acceleration time, then the time variation of the minimum energy gain per turn required to barely sustain the electrons in the design equilibrium orbit would be a decreasing sinusoid; however, as a result of energy losses by radiation, the time variation of the required minimum energy gain per turn turns out²⁵ to have a roughly constant value for about 6000 microseconds and then to decay to zero along an approximately parabolic path for the last 4500 microseconds.

* The electrons lose about 6 Mev ²⁴ in collapsing from the radius of the design equilibrium orbit to the radius of the target.

Before the advent of the spread-out beam ejection of electrons from the equilibrium orbit was accomplished by suddenly turning off a constant amplitude radio frequency accelerating voltage when the magnetic field at the equilibrium orbit had reached its peak value. As soon as the envelope of the r.f. accelerating voltage fell below that minimum value required to barely sustain the electrons in the design equilibrium orbit, the radius of the equilibrium orbit would shrink; consequently the electrons would suddenly spiral inward to strike the 0.020 inch thick platinum target placed inside the quartz vacuum chamber of the machine. The beam pulse duration corresponding to the length of time that the electrons strike the target, was observed to be about 10 microseconds on a photon beam monitor oscilloscope. The duty cycle (i.e. the fraction of the time that the beam exists) for a 10 microsecond beam pulse, which occurs six times per second, is 0.006 percent.

If the resolution time of the coincidence counting arrangement is small compared to the duration of a beam pulse, then the ratio of the real counting rate to the accidental counting rate is increased by using a beam pulse of longer duration. This improvement in the ratio of "reals" to "accidentals" occurs because the accidental counting rate, for double coincidences, is inversely proportional to the duty cycle of the beam pulse.²⁶

A beam pulse of longer duration (i.e. one that is spread out to about 2500 microseconds) is obtained from the Berkeley synchrotron by changing the shape of the envelope or modulation of the r.f. accelerating

voltage. The time variation of the envelope is changed from an essentially square wave pulse, of width equal to the electron acceleration time of about 7900 microseconds, to a shape that roughly matches the time variation of the minimum energy gain per turn required to barely sustain the electrons in the design equilibrium orbit. The electronic circuits for shaping the r.f. envelope are described briefly in Reference 25. Further details of the r.f. system of the Berkeley synchrotron are given in Reference 24.

Electrons are accelerated during that time when the r.f. envelope is greater than the minimum energy gain per turn required to barely sustain the electrons in the design equilibrium orbit. Electrons are ejected over a period of a few thousand microseconds when the r.f. envelope is equal to or slightly smaller than the minimum energy gain per turn. These relationships are illustrated in Fig. 10.

The duty cycle for a 2500 microsecond pulse, which occurs six times per second, is 1.5 percent. This value represents an improvement by a factor of 250 over the former duty cycle of 0.006 percent for a 10 microsecond pulse.

2. The Energy Distribution of the Photons

The energy distribution of the x-rays or photons is a function of the thickness of the platinum target which is bombarded by the electrons in the Berkeley synchrotron. The theoretical differential energy spectrum which is produced by monoenergetic electrons of 322 Mev striking an infinitely thin platinum target, is shown in Curve A of Fig. 11. This

characteristic bremsstrahlung spectrum is based on the Fermi-Thomas model for the atom and the Bethe-Heitler^{27,28} bremsstrahlung theory. The calculations were made by R. Christian. This spectrum is modified by the thickness of the target as a result of the processes of multiple production of photons, multiple scattering of bombarding electrons, and absorption of the high energy photons (chiefly by the pair production process) in the platinum. The effects of each of these processes is the following. Multiple production of x-rays occurs when a single electron of exactly 322 Mev energy loses energy by a bremsstrahlung process in the field of a certain platinum nucleus; then, this same electron but now of reduced energy, again produces x-rays by another bremsstrahlung process in the field of a different platinum nucleus farther along in the target. The x-rays thus produced by such a second, third, or higher multiple bremsstrahlung process will have successively lower average energy than those x-rays produced in the original or preceding process. This lowering in average photon energy would be more marked, as first pointed out by McMillan, in connection with Reference 23, if it were not for multiple scattering of the electrons in the target. The electrons which have been multiply scattered are no longer pointing in their original direction. Calculations²³, using the multiple scattering formulas of E. J. Williams, show that the electrons are sufficiently out of line after traversing the first few mils of the platinum target so as to cause most of the photons produced by them to be removed by the primary collimator. The primary collimator utilizes only that

part of the photon beam which is contained in a cone having a half angle of about $1/2^\circ$.²⁹ The result of this multiple scattering is to give a spectrum more nearly like that for an infinitely thin target. Since the spectrum comes almost entirely from the first four or five mils of the target, these quanta will be absorbed, chiefly by pair production, in passing through the remaining three quarters of the target. The magnitude of these corrections to the bremsstrahlung distribution have been tabulated in Reference 23. The calculated differential energy distribution for a 20-mil thick platinum target is shown in Curve B of Figure 11. The results of the calculations show that absorption in the target removes only about 10 percent of the quanta, and that the absorption coefficient changes by only 12 percent over the energy range from 40 Mev up to 322 Mev. The correction is practically a constant one which reduces the intensity almost uniformly by about 10 percent.

The method of producing the "spread-out" photon beam causes the electrons, which strike the platinum target, to have a distribution of energies. The origin of this energy distribution is easily explained with the aid of Figure 10. At the beginning of the ejection time t_1 , electrons of energy E_1 spiral inward to strike the platinum target. At some later time, say t_2 , electrons of higher energy E_2 are ejected from the design equilibrium orbit; and at the particular time t_3 , electrons of maximum energy E_{\max} are ejected. For ejection times later than t_3 , electrons of energy smaller than the peak energy are ejected.

The theoretical bremsstrahlung energy distribution for monoenergetic electrons striking a 20 mil thick platinum target, Curve (B) of Figure 11, must be further corrected for the variation in electron beam energy and intensity, which results from the production of the "spread-out" photon beam. If this correction is to be a minimum, then it is necessary that the electron beam intensity be adjusted for maximum intensity at peak energy. This adjustment is made by controlling the timing, the amplitude, and the decay shape of the envelope of the r.f. accelerating voltage so that the photon beam pulse is centered about the time of peak magnetic field. The time of peak magnetic field is, in turn, determined by an electronic peak field indicator, which is accurate to better than plus or minus 100 microseconds.³⁰ Since electron beam intensity and photon beam intensity are proportional to each other, the energy distribution of the electron beam can be determined from (a) the known (Curve A, Figure 11) time variation of the energy of the electrons in the design equilibrium orbit, (b) a photograph of the time variation of the photon beam intensity, and (c) a fiducial time marker, superimposed on the photograph, to indicate the occurrence of maximum electron energy. Integration of the bremsstrahlung spectrum over this electron energy distribution gives a resultant spectrum that is corrected for the "spread-out" photon beam.

3. The Collimation

a. The Primary Collimation

The x-rays, which are produced as a result of the bremsstrahlung

process at the platinum target, pass through 1.5 to 2.0 cm of quartz before reaching the air where practically all experiments are performed. The photons are emitted in a narrow cone which has a full width, at half intensity, of 0.0135 radians.²⁹

The beam is collimated by means of a tapered hole in a lead wall, 9-1/2 inches thick. The distance of the platinum target from the nearer edge of this lead wall is 55 inches. The size of the primary collimator is specified by the entrance diameter of the collimator hole. The exit diameter of the primary collimating hole is larger than the entrance diameter; the amount of taper is designed to correspond to the taper of the beam cone. In these experiments, the entrance diameter of the primary collimator was selected to be one-half inch. A one-inch diameter collimator gave rise both to chance coincidences and also to a low ratio of the counting rate with the target in the beam to the counting rate with the target removed; a smaller collimator would reduce the real counting rate.

b. The Secondary Collimation, and the Shielding of the Counters

The principles of the secondary collimation and of the shielding of the counters, which were employed in this experiment, are illustrated in Figure 12.

The secondary collimation is designed to minimize the effect of the beam spray on the counting apparatus. This beam spray consisting of photons, electrons and positrons, is created at the walls of the primary collimator, for example, when these walls are struck by those

photons which lie outside a cone having a half angle of about $1/2^{\circ 29}$. Many such photons are produced, as discussed earlier, as a result of the multiple scattering of the electrons in the platinum target. In fact, multiple scattering calculations²³ show that the electrons are sufficiently out of line after traversing the first few mils of the platinum target so as to cause most of the photons produced by them to be removed by the primary collimator. An oversize secondary collimating hole (three inches in diameter), in an 8 inch thick lead wall, is chosen in order to insure that the most intense part of the beam will not strike the walls of this secondary collimator. Since only the halo around the beam and only some of the beam spray created at the primary collimator can strike the walls of secondary collimator, and since the intensity of this halo and this beam spray is very much reduced compared to the main part of the beam, then the background at the counter positions with the target out of the beam is lowered considerably by such a secondary collimator.

Further improvements in the reduction of background were made by using lead brick shielding of the scintillation counter telescopes. The lead bricks were located in such a way that neither telescope could "see" any point of the walls of the three inch hole in the secondary collimator. In addition, since coincidences between telescopes represent the real effect, care was taken to insure that no lead brick could be seen by both telescopes at the same time.

4. The Integration of the Beam Intensity

Three different sets of beam integration equipment exists, at present, at the synchrotron. The measured unit of integrated beam is specified differently for each integrating device. A pre-collimator ion chamber and so called "Nunan meter" recorder measures "pre-collimator Nunans". A portable ion chamber and Nunan meter recorder measures "portable Nunans". Another pre-collimator ion chamber and integrating electrometer measures "integrator volts". Each of these recording devices can be calibrated³¹ in terms of "equivalent quanta". The number of "equivalent quanta", Q is defined³² as the total energy in the beam divided by the maximum photon energy of the bremsstrahlung spectrum.

The reading of the pre-collimator Nunan meter was used as the standard beam monitor reading in this experiment. The constancy of the ratio of either the number of "portable Nunans" or the number of "integrator volts" to the number of "pre-collimator Nunans" served as a check on the reading of the pre-collimator Nunan meter.

5. The Alignment of the Experimental Apparatus with the Direction of the Photon Beam

The target, the secondary collimation, and the reference angles of zero degrees for protons and 180 degrees for pions were aligned with the beam direction by means of a transit. The alignment of the experimental apparatus with the beam direction was confirmed by taking photographs of the beam at the secondary collimator ahead of the target, at the target, and at the position of the zeus meter some distance behind the target. The beam photographs showed that the diameter of the photon beam at the target was about $1\frac{1}{4}$ inches.

B. The Target

1. Choice of Heavy Water; Subtraction of Background by Using Ordinary Water

A target of free neutrons at rest does not exist because of the well known difficulties of "bottling" neutrons. Further, even if free neutrons could be "bottled", the fact that a free neutron is beta unstable against decay into a proton plus an electron plus a neutrino, with a mean-life of about 20 minutes,³³ prevents the use, in principle, of a "bottle" or target of uncontaminated free neutrons at rest. Instead, a supply of nearly free neutrons is found in deuterium nuclei. The very loosely bound neutron in the beryllium nucleus can also be considered for the target.

A target of heavy water, which contains deuterium nuclei in chemical combination with oxygen nuclei, was chosen to be studied first chiefly because the background processes could be subtracted out in an understandable and unambiguous way by simply replacing the heavy water with ordinary water. A significant difference in the counting rates from heavy water and ordinary water, if such a difference is found to exist, is not likely to be the result of the difference in the binding of the protons in heavy water and in ordinary water. Thus, the existence of a heavy water-ordinary water difference counting rate would almost certainly be attributed to the neutrons in the deuterium nuclei.

The availability and the simplicity of handling were two other factors in favor of choosing heavy water and ordinary water targets.

2. Thickness

The thickness of the target was chosen to roughly maximize the ratio of the expected counting rate for pion-proton coincidences to the expected background counting rate. The thickness of 1.50 centimeters was necessarily the result of a compromise between the two contradictory requirements. An increase in the target thickness would increase the production probability of real processes in proportion to the increased thickness; however, the detection efficiency will decrease if the target is made too thick. The detection efficiency is defined for a given geometry as that detectable fraction of real processes. For a pion-proton coincidence to be recorded, it is necessary that each particle can leave the target, in the direction of the detector, with an energy equal to or greater than the telescope detection threshold for that particle. For example, if the ionization loss in the target degrades the proton energy to a value just below the proton detection threshold of approximately 20 Mev, then a further increase in a target thickness will not result in any more real counts, but will result only in an increase in the number of background processes produced. Indeed, the energy loss of the protons, rather than the pions, in the material of the target limits the target thickness for this experiment.

The detection efficiency for protons may be divided into two parts: one part which depends upon the target thickness and one part which does not. The target independent part is a function of the

geometry and of the properties of the proton detector. The target dependent part of the detection efficiency for protons depends on the target thickness and the proton production kinetic energy through the range-energy relation for protons. The proton production kinetic energy depends, in turn through the conservation laws, on both the proton angle and the photon energy.

The target dependent part of the proton detection efficiencies, at some representative proton angles, and for some representative photon energies, are plotted in Figure 13 against target thickness in centimeters of water. These plots were obtained from the curves of Figure 14 under the assumption that multiple scattering of protons is negligible. For target thicknesses greater than about 1.00 cm and for photon energies smaller than about 220 Mev, the target dependent part of the proton detection efficiency is no longer a function of the proton angle, but is now determined by the detection threshold of approximately 20 Mev of the proton detector. Within these limits of target thicknesses and photon energies, the independence of the target dependent part of the proton detection efficiency on proton angle occurs at values of proton angles smaller than about 20° .

The information contained in Figure 14 was obtained as follows: The curves of proton kinetic energy after absorption in water versus proton kinetic energy were computed with the aid of the range-energy relation for protons in water.³⁴ The curves of proton angle versus proton kinetic energy for various photon energies were computed from

the conservation laws for the photoproduction of a negative pion from a free neutron at rest. The meaning of the composite plot may be illustrated by the following example. A 220 Mev photon produces a 33 Mev proton at an angle of 30° . Now a 33 Mev proton can be degraded in the target to an energy just below the proton detection threshold of about 20 Mev before it will fail to be detected in the proton telescope. The graph shows that target thicknesses greater than about 0.6 cm reduces the proton energy to values smaller than the 20 Mev detection threshold of the proton telescope.

The composite plot (Figure 14) for protons is useful for calculating absorber thicknesses for the proton telescope. A similar composite plot (Figure 15) for pions is useful for calculating absorber thicknesses for the pion telescope.

For simplicity, the above discussion has concerned the free neutron at rest. The modifications resulting from the momentum distribution of the deuteron neutrons have been calculated for use in the experiment.

3. Orientation

The optimum proton detection efficiency for a fixed target thickness of 1.50 centimeters was utilized by orienting the plane of the target perpendicular to the direction of the proton momentum. This particular choice of target orientation also increases the effective target volume without decreasing the proton detection efficiency. The effective target volume is defined as that volume which is common to

the target and to the photon beam. For such a choice of target orientation, the effective target volume is the volume of an oblique cylinder, which has a base area given by the projected area of the beam on the target plane, and which has a height given by the target thickness; furthermore, the projected area of the beam on the target plane depends on the particular value of the proton angle. To the approximation that the oblique cylinder is circular and not elliptical, the effective target volume is given by

$$V = \frac{A}{\cos X} d,$$

where A = the cross sectional area of the photon beam,
 X = the proton angle, and
 d = the target thickness.

Also, in this approximation, the effective target volume may be written

$$V = A l_k^{\wedge}, \quad \text{where } l_k^{\wedge} = \frac{d}{\cos X}.$$

The quantity l_k^{\wedge} is a length, measured in the direction of the photon momentum vector k , which represents the effective thickness of the target presented to the beam. Since the expected counting rate is directly proportional to the effective target volume, this length may be used as an approximate, but simple and quick measure of the change in the expected counting rate with target orientation.

4. Containers

The identical containers for the heavy water or for the

ordinary water had a drum-type construction. Each container was made out of a cylindrical brass ring, having a length of 1.5 centimeters, an inside diameter of 3-3/4 inches and an outside diameter of 4 inches. Thin 0.002 in. aluminum foils were stretched tightly across the top and bottom faces of the brass ring and then secured to the ring with araldite.* Special care was taken in the process of sealing with araldite to insure that there would be no bulging of the aluminum foils when the container was filled with water. Each filled container was optically tested for the existence of any such bulging effect; no noticeable bulging was found on any of the targets. Furthermore, the heavy water and the ordinary water were interchanged between two containers during some of the bombardments; no bulging effects were detectable within the statistical accuracy obtained.

5. The Reduction of Systematic Errors

The cylindrical targets of heavy water and ordinary water were interchanged successively during the bombardment in order to reduce the systematic errors caused by voltage drift of the electronic equipment and by variations in photon beam intensity from the synchrotron.

C. The Scintillation Counter Telescopes

1. The Two Experimental Arrangements

The scintillation counters employed detect the passage of

* Araldite is the trademark of the Ciba Company, Inc., 627 Greenwich Street, New York 14, N.Y., for a class of hardenable resins called Ethoxylines.

charged particles through stilbene phosphors. One scintillation counter telescope defines the proton angle; another, the pion angle. Two different experimental arrangements were used.

In the first experimental arrangement, each telescope consisted of two stilbene scintillation phosphors. The four counters were connected in quadruple coincidence.

In the second experimental arrangement, a third scintillation counter was added to each telescope and was connected in anti-coincidence with the output of the quadruple coincidence of the first two counters in each telescope. The purpose of the third counters is to further discriminate against background by taking advantage of the energy correlations of the photo-pion production process from a very loosely bound neutron in deuterium. The production of negative pions and protons from the tightly bound neutrons in oxygen will have (1) a smaller probability of satisfying both the required energy and angular correlations simultaneously than the production from a nearly free neutron will have, and (2) a smaller probability of satisfying both the required energy and angular correlations simultaneously than of satisfying only the angular correlation condition. For example, if either the pion or the proton has enough energy to cause a pulse in the third or anti-coincidence counter in each telescope, then the quadruple coincidences between the first two counters in each telescope is not recorded on that particular scalar which is reserved for processes surviving anti-coincidence. No information is discarded by the use of this anti-coincidence arrangement

because another scalar records at the same time all of quadruple coincidences that occur between the first two counters of each telescope.

2. The Telescope Geometries

a. Areas of the Phosphors

All the phosphors had an area of about 2 in. x 1-3/4 in. and were oriented with the larger dimension perpendicular to a horizontal plane. This plane contains the photon momentum vector and both the pion and proton momentum vectors for the photoproduction process from a free neutron at rest.

b. Designations of the Phosphors

The counters were designated with the notation P1, P2, P3, π 1, π 2, and π 3, where the letter "P" designates the proton telescope and the letter " π " designates the pion telescope, and where the numbers 1, 2, and 3 designate the first, second, and third counters in the order met by the particle entering the telescope.

c. Thicknesses of the Phosphors

The thicknesses of the phosphors are given in Table I:

TABLE I

<u>Phosphor</u>	<u>Thickness (Inches)</u>	<u>Thickness (gm/cm²)</u>
P1	1/16	0.260
P2	1/8	0.6
P3	1/8	0.6
1	3/8	1.2
2	3/4	2.4
3	3/8	1.2

The thicknesses of the phosphors were not very critical except for the thickness of the front phosphor in the proton telescope. The detection threshold of the proton telescope was essentially controlled by the thickness of the front phosphor. To minimize this detection threshold, the front phosphor was carefully sanded down to the thickness of 260 mg/cm^2 .

d. Spacings between the Phosphors

Unless otherwise specified, the spacing between the phosphors was about $1\text{-}5/8$ in. The geometry of the scintillation counter telescopes is illustrated in Figure 16.

e. Mounting of the Phosphors

In order to improve the light collection efficiency of the stilbene scintillation counters, all surfaces of each stilbene phosphor, except the surface facing the photocathode of the photomultiplier tube, were wrapped with a very thin (0.0005 in.) aluminum foil. The aluminum foil functioned as a light reflecting back surface for the stilbene phosphors. The phosphors, with their aluminum reflecting foils, were secured with two layers of black photographic tape to a magnetic shield, which fits over the LP21 type photomultiplier tubes. A window in the magnetic shield allowed the light to reach the photocathode of the photomultiplier tube. Two layers of black photographic tape were used to insure a light tight seal around the phosphors and at the junction of the phosphors with the magnetic shields.

The very thin, 260 mg/cm^2 , stilbene phosphor required some special handling and mounting precautions. A lucite frame was designed for holding and protecting the thin phosphor. The phosphor and aluminum foil assembly was allowed to slide in grooves in the lucite mounting posts, which were fastened to the magnetic shield. The two layers of photographic tape, required for a light tight seal, were wrapped around the lucite frame.

3. The Proton and Pion Detection Thresholds

The detection threshold of a two counter proton telescope, with a 260 mg/cm^2 front phosphor, is calculated from the range-energy relation for protons in stilbene³⁵ to be about 20 Mev, if the proton losses about 3 Mev before coming to rest in the P2. Two layers of black photographic tape have a measured thickness of 45 mg/cm^2 ; a stilbene equivalent of 50 mg/cm^2 for each two layers of black photographic tape plus one 1/2 inch aluminum foil was used in calculating the energy thresholds. Similarly, the detection threshold of a two counter pion telescope, with a 3/8 in. stilbene phosphor for π_1 , is calculated to be about 15 Mev if the pion loses at least 4 Mev before coming to rest in π_2 .

D. The Absorbers

1. The Choice of Materials

Copper was chosen for the material of the absorbers in the pion telescope. An absorber material such as copper, which has a large stopping power per unit length and a low atomic number, introduces a minimum of multiple scattering of the pions; on the other hand if the

cross section for nuclear interactions of pions is equal to a nuclear area, then an absorber material such as lead which has a large stopping power per unit length and a high atomic number, introduces a minimum of nuclear interaction. The stopping power per unit length is slightly greater for copper than for lead. Furthermore, copper is much less efficient than lead as a converter of high energy photons into a source of background electrons.

Aluminum was selected for the material of the absorbers in the proton telescope. Since the proton telescope is confined to the forward direction, a smaller background of fast electrons from the processes of bremsstrahlung and pair production will be created in an absorber material of low atomic number than in an absorber material of high atomic number. In addition, the stopping power per unit length of aluminum resulted in convenient absorber thicknesses for the geometry of the proton telescope.

2. The Selection of Thicknesses

For a given pair of correlation angles in the second experimental arrangement, proper thickness absorbers were introduced into both telescopes simultaneously in such a way that the target dependent part of the proton detection efficiency had (1) a fairly uniform value above a certain minimum photon energy, and (2) a zero value below this same photon energy. Discrimination against photon energies, which are smaller than the selected minimum, is accomplished by choosing the absorber thicknesses in the following way. The aluminum absorber in

the proton telescope is selected to accept protons that are produced by 260 Mev photons, say, at the edge of the target farthest away from the proton telescope; simultaneously, the copper absorbers in the pion telescope are selected to accept pions that are produced also by 260 Mev photons at the edge of the target farthest away from the pion telescope. The degree of discrimination against photons of energy lower than 260 Mev is illustrated in Figure 17.

The energies of the particles, which were detected in each telescope, were determined from range-energy curves. The range-energy curves for protons in stilbene and for pions in copper and stilbene were computed from the proton-range energy curves of Aron et al.³⁵

E. The Angular Resolution

1. Effect of the Finite Size of the Target and of the Detectors

One scintillation counter telescope defines the proton angle; another defines the pion angle. The planar angular resolution of a telescope is here defined for the photo-pion production process from a free neutron at rest in the laboratory as that angular interval, measured in the plane of the process, which is intercepted by the telescope. The smaller the angular interval intercepted, the better is the resolution. The planar angular resolutions of the two telescopes were adjusted to be equal in the center of mass coordinate system. This adjustment was made in the laboratory by simply choosing the ratio of the mean distances of the telescopes from the target such that the two telescopes would intercept equal arcs. This condition of equal arcs means that

$$\frac{r_p}{r_\pi} = \frac{\Delta\theta}{\Delta\chi}$$

where r_p = the mean distance of the proton telescope from the target,
 r_π = the mean distance of the pion telescope from the target,
 $\Delta\theta$ = the angular interval, measured in the plane of the process,
which is intercepted in the laboratory by the pion telescope, and
 $\Delta\chi$ = the angular interval, measured in the plane of the process,
which is intercepted in the laboratory by the proton telescope.

Now, the ratio $\frac{\Delta\theta}{\Delta\chi}$ is obtained from the slope of the curve (Figure 3) of pion angle versus proton angle. For the conditions of this experiment, the slope is about 2.5; hence the condition of equal planar angular resolutions in the center of mass coordinates corresponds in the laboratory to a planar angular resolution for the proton telescope which was about 2.5 times better than that for the pion telescope.

The mean distance of the pion telescope from the target was chosen to be approximately seven inches; consequently, that of the proton telescope was about seventeen inches. These values represented a suitable compromise between counting rate and angular resolution. Background and the resulting secondary collimation were also a factor in determining the minimum distances from the target.

The effect of the finite size of the target on the planar angular resolution was calculated by means of the Faltung³⁶ integral. Both a simple rectangle and a sinusoid were used to represent the target "window". The sinusoid is the result of assuming a beam of

circular cross section and of uniform intensity. A rectangular "window" represented the telescope detector in each case. The result of the folding operation in each case gave essentially the same full width at half maximum, which was about seven degrees for the proton telescope for the geometry of the experiment. Approximately this same value is obtained for the proton angular resolution by simply calculating the angle subtended by the proton detector when the target is considered as a point source. A seven degree proton angular resolution in the laboratory corresponds to an angular resolution of about seventeen degrees for either detector in the center of mass coordinates. The laboratory pion angular resolution is also about seventeen degrees.

2. Effect of Multiple Scattering in the Target

The effect on the angular resolution of multiple scattering in the target can be considered to be negligible. This result was obtained in the following manner. The geometrical angular resolution curve, which was obtained as a result of the folding operation described above, was replaced by a gaussian curve of equivalent half-width.

The root mean square value $\sqrt{\langle \theta^2 \rangle}$, of the projection of the total multiple scattering deflection angle on a plane containing the initial trajectory was found to be slowly varying over the thickness of the target. This slow variation is expected because the telescope detection thresholds require higher production energies for greater target thicknesses. Further, for the worst possible case, determined

by the experimental arrangements, the largest value of $\sqrt{\langle \theta \rangle^2}$ was less than 0.003 radians. This value was used in the gaussian distribution function for multiple scattering. The result of folding these two gaussian curves together showed that the full width at half maximum of the resulting gaussian that represents the effect of multiple scattering on the angular resolution differs by less than 4 percent from the full width at half maximum of the gaussian curve that represents the angular resolution without multiple scattering.

F. The Electronic Instrumentation

1. A Descriptive Survey

a. Introduction

A brief description of the scintillation counting equipment, which made this experiment possible, will be described here. Since this electronic development work may be useful for performing other counting experiments with beams from pulsed accelerators that have short duty cycles, a more detailed report will be prepared for later publication.

b. The Block Diagrams of the Two Experimental Arrangements

Figure 18 is a block diagram of the electronics that was used in the first experimental arrangement; Figure 19 is the corresponding diagram for the second experimental arrangement.

c. The Photomultiplier and Limiter Circuit

The same photomultiplier and limiter circuit was employed in both experimental arrangements for shaping the scintillation counter

pulses. Figure 20 is the schematic circuit diagram of the photomultiplier and the limiter; Figure 21 is the assembly drawing. Morton³⁷ discusses photomultiplier circuitry and recommends the use of an electrostatic shield for the type 1P21 photomultiplier. The pulse shaping is described in section F2.

d. The Coincidence Circuits

The coincidence circuits are modified versions of the fast coincidence circuit described by Garwin.³⁸ Figure 22 is the schematic circuit diagram of the quadruple coincidence circuit that was used in the first experimental arrangement. The quadruple coincidences were made in the second experimental arrangement by making another fast double coincidence between the fast outputs of two other double coincidence circuits. Figure 23 is the schematic circuit diagram of these double coincidence circuits.

An important addition to the Garwin type circuit is the manner in which the coincidence pulse is taken off the plates of the coincidence tube or tubes. Ragent³⁹ introduced the series connected crystal diode and resistor combination, which functions to improve the discrimination ratio of quadruple coincidences to triple coincidences.

e. The Phase Inverting Distributed Amplifier

Since the coincidence circuits require negative input pulses of about two volts amplitude, a signal polarity inverting distributed amplifier is required between the limiter output and the input to the coincidence circuit. Either the Hewlett Packard Company Model 460 B

or a phase inverting version of the Model 460 A distributed amplifier was used. The phase inverter that was introduced into the Model 460 A amplifier is shown schematically in Figure 24.

f. The Overall Performance of the Counting System

The properties of these electronic circuits which are important for discriminating against background are (1) the fast resolution time for quadruple coincidences of about 2×10^{-8} seconds, (2) the absence of dead time, and (3) the high discrimination ratio, of quadruple coincidences to triple coincidences, of greater than 16 to 1.

2. The Shaping of the Scintillation Counter Pulses

a. The Pulse Shaping Problem

The pulse shaping problem can be understood by considering the stilbene phosphor and photomultiplier combination as a pulse current generator with an internal impedance that is large compared with the load impedance. Since the amplitudes of the pulses that are delivered to the load impedance depend upon the energy that is lost by the particle in passing through the stilbene phosphor; the consequent large variations in pulse amplitudes give rise to large variations in the time that is required for the pulse amplitude to decay below a certain value. The time for the pulse amplitude to decay below that particular value which will allow the counter to accept another pulse is a measure of the "dead time" of the counter.

b. The Two Limiter Solution to the Pulse Shaping Problem

(1) The Functions of the Limiters

A solution to the pulse shaping problem is contained in

the limiter circuit (Figure 20). The limiter here limits the pulses both in duration as well as in amplitude. The short length of high impedance RG65/U delay cable serves as the time "clipper"; the sharp grid cutoff characteristic of the type 6AH6 pentode is used to limit the amplitude of the negative pulses.

The importance of the pulse duration limiter stems from its function as a "dead time" equalizer for the varying length pulses. The "dead" time of the counter is defined here as the length of time that elapses between responses of the counter to successive pulses. Short "dead time" counting circuits are especially important for discriminating against background from pulsed accelerators that have short duty cycles.

In addition to generating pulses of uniform amplitude, the function of the pulse amplitude limiter is to prevent large pulses from introducing a "dead time" into the distributed amplifier. The time constant, which is associated with the grid biasing arrangement at the receiving end of the grid line of these amplifiers, is of the order of 2 microseconds. Since this time constant is large compared to the pulse duration, a "dead time" will be introduced into the counting system if these distributed amplifiers are driven too far beyond saturation.

(2) The Design Considerations

The value of the resistor R12 is a compromise between the requirements for the pulse amplitude limiter and the pulse duration

limiter: The most effective pulse amplitude limiting occurs at large output voltages from the photomultiplier tube. For a fixed operating voltage on the photomultiplier, and for a given energy loss in the stilbene phosphor, the output voltage from the photomultiplier usually can be increased by increasing the load impedance.

The transmission line type pulse duration limiter should be terminated at its sending end in its characteristic impedance. Thus, the limit to increasing the size of the load resistor R12 was imposed by the value of the characteristic impedance of the cable. The RG65/U cable is a high impedance cable of special design;^{40,41} the characteristic impedance is specified to be 950 ± 50 ohms.

The decay time of the pulses, which are generated by the stilbene phosphor and photomultiplier combination, is smaller than the length of the clipping line. Thus, a short circuited receiving end of the line would reflect back the full amplitude of the original pulse, with a 180° phase change, so that the resultant "clipped" pulse at the sending end would have considerable "overshoot". That is, the addition of the transmitted and reflected pulses results in a "clipped" pulse of the same polarity as the original pulse but also with a sizeable contribution of the opposite polarity. Thus, the cable is terminated at its receiving end with a resistance that is small compared to the characteristic impedance of the line in order that only a fraction of the amplitude of the original pulse is reflected back, with a 180° phase change, toward the sending end. The value of this terminating resistance was selected experimentally for minimum "overshoot".

V. THE RESULTS

The following results are presented as evidence for the observation of the photo-pion production process $\gamma + n \rightarrow \pi^- + p$, by the method of pion-proton coincidences.

A. The Angular Correlations

The difference in the quadruple coincidence counting rates from heavy water and ordinary water targets has a well-defined peak. This peak occurs at those pairs of correlation angles which are predicted for the photo-production of a negative pion from a free neutron at rest. When the angle of the proton telescope is varied on either side of the predicted correlation angle, by an amount equal to the angular resolution of the proton telescope, the heavy water-ordinary water difference counting rate essentially disappears.

The experimental results that have been obtained with the second experimental arrangement are plotted in Figures 25 and 26 for pion angles of 90° and 120° with correlated proton angles of 31.5° and 20° respectively. Figures 25 and 26 show both the contributions from photon energies in the interval from 260 Mev to 300 Mev and from 260 Mev to the upper energy limit of the bremsstrahlung spectrum. The results from the two different photon energy intervals are plotted side by side in these two figures in order to invite comparison of the second experimental arrangement with the first. The counting rates obtained from heavy water and ordinary water separately, before subtraction, are plotted in Figures 27, 28, 29 and 30. Figures 27 and 28

show the contributions from photon energies in the interval from 260 Mev to 300 Mev; whereas, Figures 29 and 30 show the contributions from photon energies from 260 Mev to the upper energy limit of the bremsstrahlung spectrum. The degree of improvement in the statistical accuracy which is obtained by the use of the anti-coincidence feature in the second experimental arrangement may be seen by comparing the two figures.

B. The Energy Correlations

Within experimental error, the measured upper limit of the energy (at a given angle) of the particles entering the pion telescope agrees with the value calculated from the energy momentum conservation laws for the assumed two-body process. Similarly, agreement is obtained for the proton telescope. For example, the conservation laws predict that a 280 Mev photon will produce a negative pion with 74 Mev kinetic energy at a pion production angle of 107.5° . When a copper absorber, of sufficient thickness to stop pions that are produced at the target center with kinetic energies less than or equal to 74 Mev, is introduced into the pion telescope, then the heavy water-ordinary difference counting rate is reduced greatly. The relative counting rates are tabulated in Table II.

Similarly, the conservation laws predict that a 320 Mev photon will produce a proton with 90 Mev kinetic energy at the correlated proton angle of 25° . When an aluminum absorber, of sufficient thickness to stop protons that are produced at the target center with kinetic energies less than or equal to 90 Mev, is introduced into the proton telescope, then the heavy water-ordinary water rate practically vanishes. The relative counting rates are tabulated in Table II. The fact that any

TABLE II

EXPERIMENTAL RESULTS ON ENERGY CORRELATION & CO-PLANARITY

ARRANGEMENT	COUNTING RATES			ABSORBERS & PHOTON ENERGY LIMITS			
	D ₂ O COUNTS/INTEGRATED BEAM UNIT (DECINUNAN)	H ₂ O	DIFFERENCE	PROTON TELESCOPE		PION TELESCOPE	
				ABSORBER GMS/CM ²	PHOTON MEV	ABSORBER GMS/CM ²	PHOTON MEV
NORMAL							
FOR $\theta = 107.5^\circ, \chi = 25^\circ$	$.49 \pm .03$	$.20 \pm .02$	$.29 \pm .04$	1.95 Al	>260	NONE	>190
ABSORBER IN PROTON TELESCOPE	$.04 \pm .02$			8.2 Cu	>320	NONE	>190
ABSORBER IN PION TELESCOPE	$.21 \pm .04$	$.13 \pm .05$	$.08 \pm .06$	NONE	>220	230 Cu	>280
PION TELESCOPE TILTED AT 22°	$.08 \pm .04$			1.95 Al	>260	NONE	>190

MU 2941

residual counting rate exists at all is because some protons, which are produced near the edge of the target closest to the proton telescope, will have enough energy to get through the absorber.

The data obtained with the second experimental arrangement provide a demonstration of the simultaneous energy and angular correlations which are predicted from the photo-pion production process from a free neutron at rest. The absorbers were adjusted in each telescope, in the manner described in Part IV, Section A 2, such that pion-proton coincidences from the production of negative pions from photons in the energy interval from 260 Mev to 300 Mev only were recorded. The simultaneous energy correlation data is plotted in Figures 27 and 28 for pion angles of 90° and 120° with correlated proton angles of 31.5° and 20° respectively.

C. The Time Correlations

At least two ionizing particles are detected in time coincidence. The simultaneity of the two particles is ascertained only within the finite resolving time of about 2×10^{-8} seconds of the quadruple coincidence circuit used.

This piece of evidence is substantiated by the fact that the quadruple coincidences essentially disappear when the pulses from one telescope are delayed, relative to the pulses from the other telescope by an integral number of r.f. cycles of the synchrotron oscillator. The accidental counting rate increases sharply as the proton angle becomes smaller than about 20° , measured from the beam

direction. Such a behavior is expected because of the increased production of background events at small angles in the forward direction. The accidental counting rate that was obtained from a heavy water target is plotted for comparison in Figure 30.

D. The Co-Planarity

Within experimental error, the process is co-planar. The heavy water-ordinary water difference counting rate essentially disappears when the pion telescope is tilted out of the plane containing the photon beam and the proton telescope. The test for co-planarity was made with the first experimental arrangement under the following conditions: (1) The angle of the pion telescope was at 107.5° . (2) The angle of the proton telescope was at the correlated angle of 25° . (3) An aluminum absorber, of sufficient thickness to stop protons that are produced at the target center with kinetic energies less than or equal to 55 Mev, was introduced into the proton telescope. (4) No absorbers were introduced into the pion telescope. For an angle of tilt of about 22° , the non-co-planar quadruple coincidence counting rate for a heavy water target was 0.08 ± 0.04 per unit integrated beam (decinunan). The co-planar heavy water-ordinary water difference counting rate, under the same conditions, was 0.29 ± 0.04 per decinunan the co-planar heavy water rate alone was 0.49 ± 0.03 per decinunan.

E. The Yield

The yield of the heavy water-ordinary water difference counting rates at the correlation angles is compatible with a photo-

pion production cross section. For example, a heavy water-ordinary water difference counting rate of about 0.07 per decinunan is measured with the second experimental arrangement when absorbers are adjusted such that only photon energies in the interval from about 260 Mev to 300 Mev contribute. If the differential cross section for the production of negative pions from a neutron in deuterium is taken to be about equal to the measured^{3,13} differential cross section for positive pion production, then a very simple calculation of the number of pions which are produced in this experiment by photons in the energy interval from 260 Mev to 300 Mev, gives an expected production rate of about 0.4 negative pions per decinunan. The expected counting rate for pion-proton coincidences will be further reduced by the product of the proton detection efficiency and the pion detection efficiency.

F. The Net Charge of the Reaction Products

The difference in the quadruple coincidence counting rates from heavy water and ordinary water targets indicates that at least two ionizing particles are produced as the result of the interaction of a photon with the neutron in the deuteron. This result specifies the net charge in the initial state to be zero; charge conservation, therefore, requires that the net charge of the products in the final state be zero.

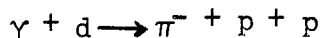
G. The Total Angular Momentum of the Reaction Products

The difference in the counting rates from heavy water and ordinary water targets requires that the total angular momentum of the reactants be half-odd integral; conservation of angular momentum, therefore, requires that the total angular momentum of the products in the final state be half-odd integral.

VI. SOME EXTENSIONS OF THE EXPERIMENT

A. The Excitation Function and the Production Cross Sections.

Scintillation counting of negative pions by the method of pion-proton coincidences should facilitate the study of the photo-pion production process from the nearly free neutron in deuterium. Both the energy and the angle of production of each particle are observable quantities in the method of pion-proton coincidences; therefore, in principle, the kinematics of the three body reaction

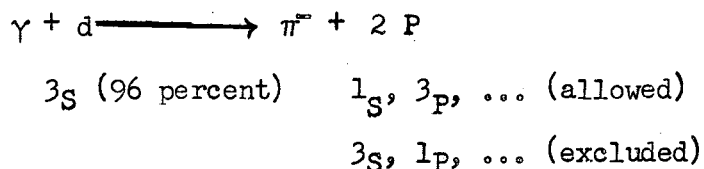


is uniquely determined. A measurement of these four quantities would yield the excitation function, the energy and the angular distributions of the negative pion production by a photon of a given energy, and, as LeLevier²¹ has pointed out, the probability that the spin of the nucleon has "flipped" (see next section) during the act of pion production.

B. The Spin-Flip Probability

The spin-flip probability is a measure of the operation of the Pauli Exclusion Principle in the photo-pion production from deuterium.

Now, consider the reaction



The deuteron is initially in the 3_S state (96 percent). Only the anti-symmetric $1_S, 3_P, \dots$ states are allowed, and the symmetric $3_S, 1_P, \dots$ states are excluded by the Pauli Exclusion Principle for the

final state of the two protons. If the spin of the target neutron in the deuteron is not "flipped" during the photo-pion production process, then the 1_S state is excluded also. Thus, the volume in phase space available for the final state of the reaction and consequently the cross section for photo pion production from a nucleon bound in the deuteron are reduced relative to that for photo-pion production from a free nucleon.

If the two protons have large relative energy, then the cross section for photo-pion production from a nucleon bound in the deuteron is not reduced very much in comparison with that from a free nucleon. If the pion is emitted in the backward direction, a study of the kinematics of the reaction shows that the two protons have small relative energy even though their absolute energy is comparatively large. For example, a 280 Mev photon produces a negative pion of about 95 Mev at a production angle of 120° and two protons, each with an energy of about 22 Mev, at production angles of 20° and 27° . On account of the small relative energy, the matrix elements for transitions to the $3P$, $1D$, ... antisymmetric states are very small compared to the matrix element for the transition to the 1_S state; hence, the experimental observation of pions of the maximum possible production energy at a given production angle must be evidence for a spin flip process. The ratio of the cross section at maximum pion energy to that at the lower pion energies, corresponding to the production from a free nucleon, should then provide a measure of the spin flip probability. LeLevier²¹

has pointed out that the magnitude of the cross section at the high energy end of the pion spectrum is a sensitive function of the high fourier components of the deuteron wave function.

It should also be pointed out that the main experimental difficulty with this experiment is detecting one or both of the protons. The proton production energy is rapidly degraded in either the material of the target or the walls of a vessel containing deuterium gas; however, there still remains the possibility, suggested by Moyer⁴², of using the gas target as a proportional counter for the proton detection.

C. Pion-Proton Coincidences from Beryllium

The production of negative pions from the very loosely bound neutron in the beryllium nucleus could possibly be investigated by studying the angular correlations of pion-proton coincidences.

D. The Artificial Production of the V^0 Particle

A search for the artificial production of the V^0 particle, which has recently been observed in the cosmic radiation, might prove fruitful. If the V^0 particle is assumed to decay into a negative pion and a proton, then the kinematics of the angular and energy correlations of the pion-proton coincidences from a V^0 particle of a given velocity is similar to the kinematics of the angular and energy correlations of the pion-proton coincidences for the photo-pion production process.

E. Momentum Distributions in Nuclei

The study of the angular and the energy correlations of

pion-proton coincidences that are produced by photons of higher energies than those from the Berkeley synchrotron should lead to information about the momentum distributions of the neutrons within the nucleus and possibly to information about the pion interaction with the nucleons of the nucleus in which the pion is produced.

F. Development of a Detector of Negative Pion "Stars"

Since there is not yet any fully developed counter technique which can positively identify a negative pion by one of its characteristic properties, such as star formation, the restriction against protons from the two-body process ($\gamma + n \rightarrow \pi^- + p$) being emitted along the direction of the meson momentum vector \vec{q} is a useful fact which simplifies the study of the mesons themselves. Perhaps, this property may permit the successful development of a scintillation counter detector of π^- stars. Such a π^- detector would permit the study of the dependence of the production cross sections on the mass number A of the target nucleus.

VII. THE ACKNOWLEDTEMENTS

I wish to express my appreciation to Professor B. J. Moyer for his continued guidance and support. I am indebted to Mr. K. C. Bandtel and to Mr. W. J. Frank for their cooperation and assistance throughout the course of the experiment. I would like to thank Mr. Edward Vaughan for helpful discussions of many aspects of this work. I am indebted to Mr. P. V. Nikonenko for the major part of the electronic engineering; to Mr. G. Culler for numerical evaluation of the calculations for the photo-pion production from a free neutron with a vector momentum. My sincere thanks go to Mr. George McFarland and to the entire synchrotron crew for their help in making the bombardments.

The work described in this paper was performed under the auspices of the Atomic Energy Commission.

VIII. THE REFERENCES

1. E. Gardner and C. M. G. Lattes. Science 107, 270 (1948).
2. E. M. McMillan and J. M. Peterson. Science 109, 438 (1949).
3. R. S. White. Ph.D. Thesis, University of California (1951)
"Photomesons from Deuterium".
4. R. M. Littauer and D. Walker. Bull. Am. Phys. Soc. 26 No. 3,
15 (1951); Phys. Rev. 82, 746L (1951).
5. K. A. Breuckner. Phys. Rev. 79, 641 (1950).
6. McMillan, Peterson and White. Science 110, 579 (1949).
7. Peterson, Gilbert and White. Phys. Rev. 81, 1003 (1950).
8. Camac, Corson, Littauer, Shapiro, Silverman, Wilson, and Woodward.
Bull. Am. Phys. Soc. 26 No. 1, 48 (1951); Phys. Rev. 82, 745 (1951).
9. M. J. Jakobson. Ph.D. Thesis, University of California (1951)
"The Production of Photomesons from Helium".
10. M. Camac. Rev. Sci. Instr. 22, 197 (1951).
11. H. A. Medicus. Bull. Am. Phys. Soc. 26 No. 3, 15 (1951);
Phys. Rev. 83, 662 (1951).
12. L. J. Cook. Private Communication.
13. J. Steinberger and A. S. Bishop. Phys. Rev. 78, 493 (1950);
Phys. Rev. 78, 494 (1950).
14. Bishop, Steinberger, and Cook. Phys. Rev. 80, 291 (1950); also
A. S. Bishop, Ph.D. Thesis, University of California (1950).
15. R. F. Mozley. Phys. Rev. 80, 493 (1950); Ph.D. Thesis, University
of California (1950).
16. Panofsky, Steinberger, and Steller. Phys. Rev. 78, 802 (1950);
UCRL-1495 (Oct. 1, 1951) (pending publication in Phys. Rev.).
17. A. Silverman and M. Stearns. Phys. Rev. 83, 206 A and 853 L (1951).
18. H. Feshbach and M. Lax. Phys. Rev. 76, 134 (1949); Phys. Rev.
81, 189 (1951).

19. G. F. Chew and G. C. Wick. (To be published in Phys. Rev.)
20. G. F. Chew and H. W. Lewis. Phys. Rev. 84, 779 (1951).
21. R. LeLevier. Private Communication; Bull. Am. Phys. Soc. 26 No. 8, 23 (1951).
22. Heckrotte, Henrich, and Lepore. (To be published in Phys. Rev.), "Neutral Photo-Meson Production in Deuterium".
23. W. M. Powell, W. Hartsough, and M. Hill. Phys. Rev. 81, 213 (1951).
24. M. H. Dazey, J. V. Franck, A. C. Helmholtz, C. S. Nunan, J. M. Peterson. Rev. Sci. Instr. 21, 436 (1950).
25. G. Gauer and C. Nunan. UCRL-714.
26. N. Feather. Proc. Camb. Phil. Soc., 45, 648 (1949).
27. H. A. Bethe and W. Heitler. Proc. Roy. Soc. 159, 432 (1937).
28. B. Rossi and W. Greisen. Rev. Mod. Phys. 13, 253 (1941).
29. J. Rose. Private Communication.
30. G. Gauer. Private Communication.
31. W. Blocker, R. W. Kenney and W. K. H. Panofsky. Phys. Rev. 79, 419 (1950).
32. E. McMillan, W. Blocker and R. W. Kenney. Phys. Rev. 81, 455 (1951).
33. J. M. Robson. Phys. Rev. 83, 349 (1951).
34. W. Aron. UCRL Engineering Note (Feb. 15, 1951), "Ranges in H₂O".
35. Aron, Hoffman and Williams. "Range Energy Curves", UCRL-121, 2nd Rev. (1949).
36. R. V. Churchill. "Modern Operational Mathematics in Engineering", McGraw Hill Book Co., Inc. (1934).
37. G. A. Morton. R.C.A. Review 10 No. 4, 525 (1949).
38. R. L. Garwin. Rev. Sci. Instr. 21, 569 (1950).
39. B. Ragent. Private Communication.

40. J. F. Blackburn. M.I.T. Radiation Laboratory Series 17, 27 (1949).
"Components Handbook".
41. H. E. Kallmann. Proc. I.R.E. 34, 348 (1946).
42. B. Moyer. Private Communication.

IX. THE ILLUSTRATIONS

- Figure 1. Angular correlation for the process $\gamma + n \rightarrow \pi^- + p$ (calculated for a free neutron at rest). Plots of proton angle versus pion angle for various photon energies from near threshold to 1000 Mev.
- Figure 2. Angular correlation for the process $\gamma + n \rightarrow \pi^- + p$ (calculated for a free neutron at rest). Plot of proton angle versus photon energy for a pion angle of 90° .
- Figure 3. Angular correlation for the process $\gamma + n \rightarrow \pi^- + p$ (calculated for a free neutron at rest). Plots of proton angle versus pion angle for photon energies of 220, 260 and 300 Mev. This plot illustrates the degree of angular correlation only over that range of proton and pion angles and photon energies which are observable in this experiment. The laboratory angular resolution of the detectors is superimposed here for comparison with the degree of angular correlation.
- Figure 4. Plot of the maximum proton angle versus photon energy for the process $\gamma + n \rightarrow \pi^- + p$ (calculated for a free neutron at rest).
- Figure 5. A vector momentum diagram, in the laboratory coordinate system, for the photo-pion production from a free neutron at rest. The laboratory pion angle is chosen greater than the maximum allowable proton angle.

Figure 6. Angular correlation in a plane for the process $\gamma + n \longrightarrow \pi^- + p$
(calculated for a free neutron with a vector momentum).

Plots of proton angle versus pion angle at a photon energy
of 300 Mev.

Figure 7. Angular correlation in a plane for the process $\gamma + n \longrightarrow \pi^- + p$
(calculated for a free neutron with a vector momentum).

Plots of proton angle versus pion angle at a photon energy
of 220 Mev.

Figure 8. A vector momentum diagram, in the laboratory coordinate
system, for the photo-pion production from a free neutron
with a vector momentum.

Figure 9. Energy correlation for the process $\gamma + n \longrightarrow \pi^- + p$
(calculated for a free neutron at rest). Lines of constant
proton angle and lines of constant photon energy are
plotted on the plane of proton kinetic energy versus pion
kinetic energy.

Figure 10. Curves illustrating the origin of the "spread-out" photon
beam from the synchrotron.

Curve (A): Time variation of the energy of the electrons
in the design equilibrium orbit.

Curve (B): Approximate time variation of the minimum energy
gain per turn required to barely sustain the
electrons in the design equilibrium orbit.

Curve (C): Time variation of the envelope of the radio
frequency accelerating voltage designed to
provide the "spread-out" beam.

Figure 11. Photon energy spectrum. The differential energy spectrum of the photons versus the photon energy. Curve (A) is for an infinitely thin platinum target; Curve (B) is for a 20 mil thick platinum target.

Figure 12. Schematic diagram of the secondary collimation and of the shielding of the counters.

Figure 13. Plots of proton detection efficiency at various proton telescope angles and at various photon energies versus target thickness.

Figure 14. Plot of proton telescope angle versus proton energy after leaving the target. This plot is a composite plot which is created by the superposition of a plot of proton telescope angle versus proton production energy and a plot of proton energy after leaving various thicknesses of target versus proton production energy.

Figure 15. Plot of pion telescope angle versus pion energy after leaving the target. This plot is a composite plot which is created by the superposition of a plot of pion telescope angle versus pion production energy and a plot of pion energy after leaving various thicknesses of target versus pion production energy.

Figure 16. Schematic diagram of the geometry of the scintillation counter telescopes.

- Figure 17. Plot of the minimum photon energy that is required to produce proton-pion coincidences for a given set of absorbers in the proton and the pion telescope versus the production position, measured along the beam direction, in the water target.
- Figure 18. Block diagram of the electronics used in the first experimental arrangement.
- Figure 19. Block diagram of the electronics used in the second experimental arrangement.
- Figure 20. Schematic circuit diagram of the photomultiplier and the limiter.
- Figure 21. Assembly drawing of the photomultiplier and the limiter.
- Figure 22. Schematic circuit diagram of the quadruple coincidence circuit that was used in the first experimental arrangement.
- Figure 23. Schematic circuit diagram of the double coincidence circuits that were used in the second experimental arrangement.
- Figure 24. Schematic circuit diagram of the phase inverter that was introduced into the Hewlett-Packard Model 460 A distributed amplifier.
- Figure 25. Plot of the difference in the counting rate from heavy water and ordinary water targets versus the proton telescope angle when the pion telescope angle is fixed at 90° .

- Figure 26. Plot of the difference in the counting rate from heavy water and ordinary water targets versus the proton telescope angle when the pion telescope angle is fixed at 120° .
- Figure 27. Plot of the heavy water counting rate and also the ordinary water counting rate from photon energies in the interval from 260 Mev to 300 Mev versus the proton telescope angle when the pion telescope angle is fixed at 90° .
- Figure 28. Plot of the heavy water counting rate and also the ordinary water counting rate from photon energies in the interval from 260 Mev to 300 Mev versus the proton telescope angle when the pion telescope angle is fixed at 120° .
- Figure 29. Plot of the heavy water counting rate and also the ordinary water counting rate from photon energies greater than 260 Mev versus the proton telescope angle when the pion telescope angle is fixed at 90° .
- Figure 30. Plot of the heavy water counting rate and also the ordinary water counting rate from photon energies greater than 260 Mev versus the proton telescope angle when the pion telescope angle is fixed at 120° . Also shown is a plot of the accidental counting rate from a heavy water target versus the proton telescope angle when the pion telescope angle is fixed at 120° .

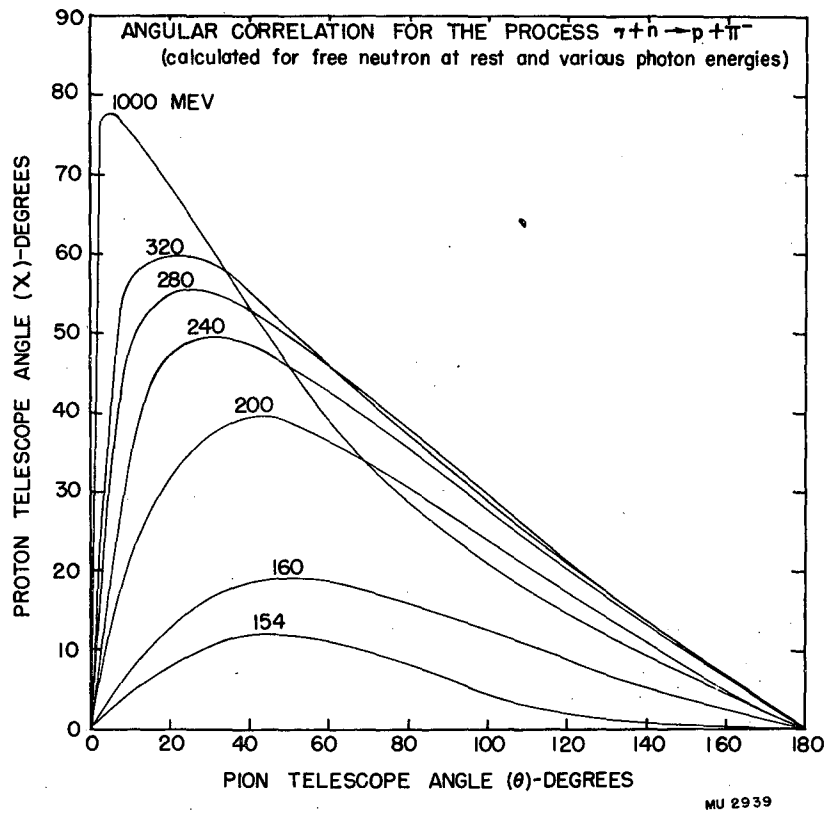
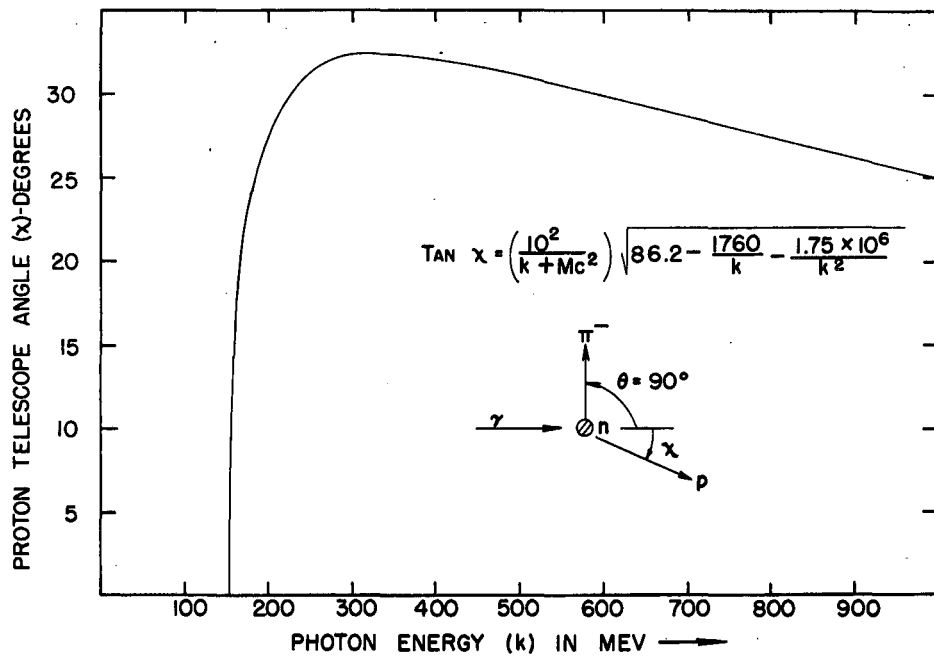


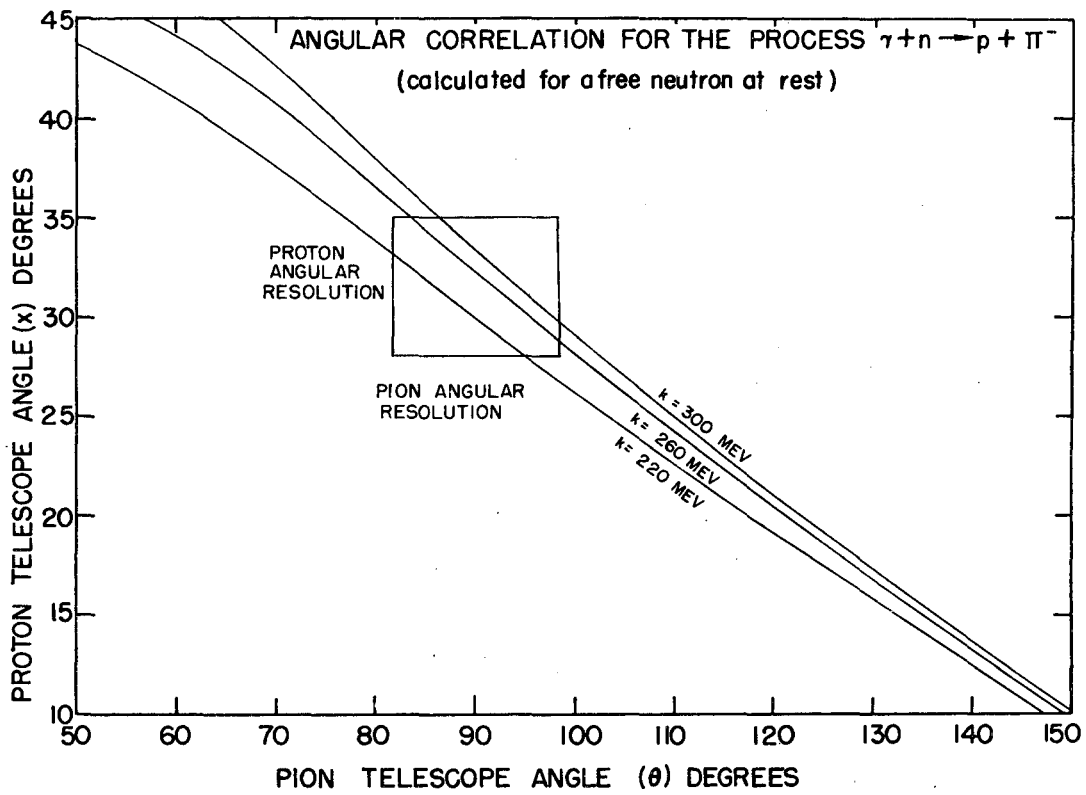
Fig. 1



PROTON ANGLE (χ) vs. PHOTON ENERGY (k) FOR THE PROCESS $\gamma + n \rightarrow \pi^- + p$
CALCULATED FOR FREE NEUTRON AT REST
PION TELESCOPE ANGLE (θ) FIXED AT 90°

MU 2936

Fig. 2



MU 2937

Fig. 3

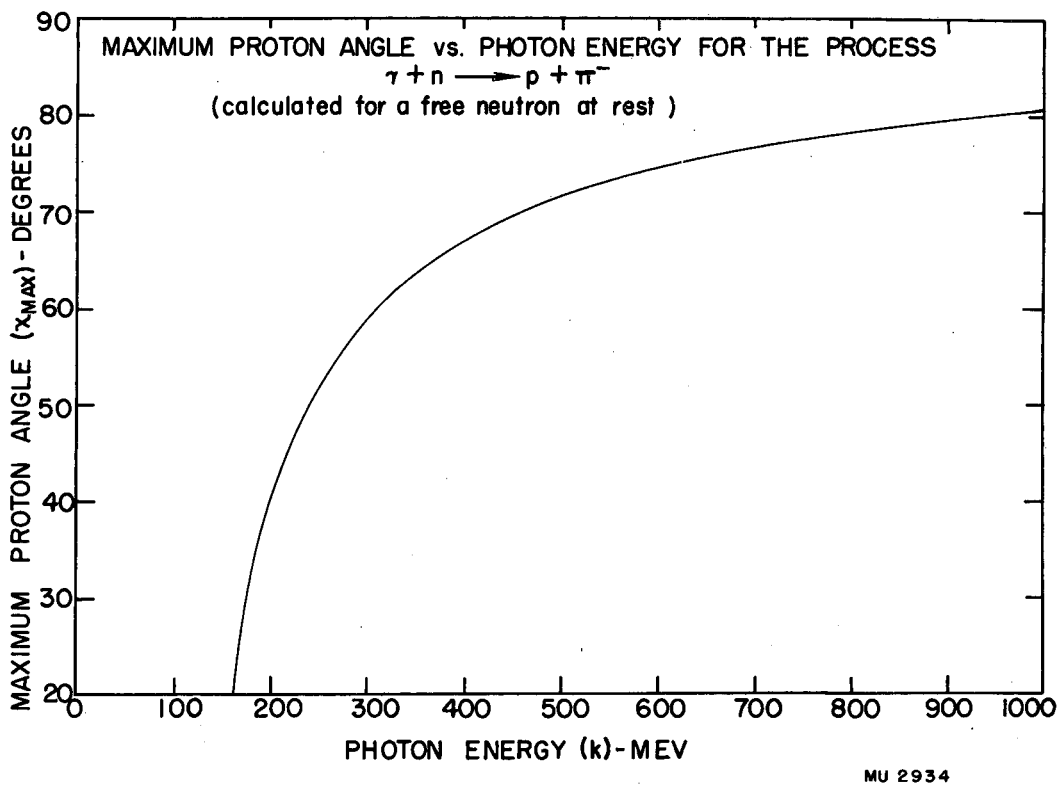
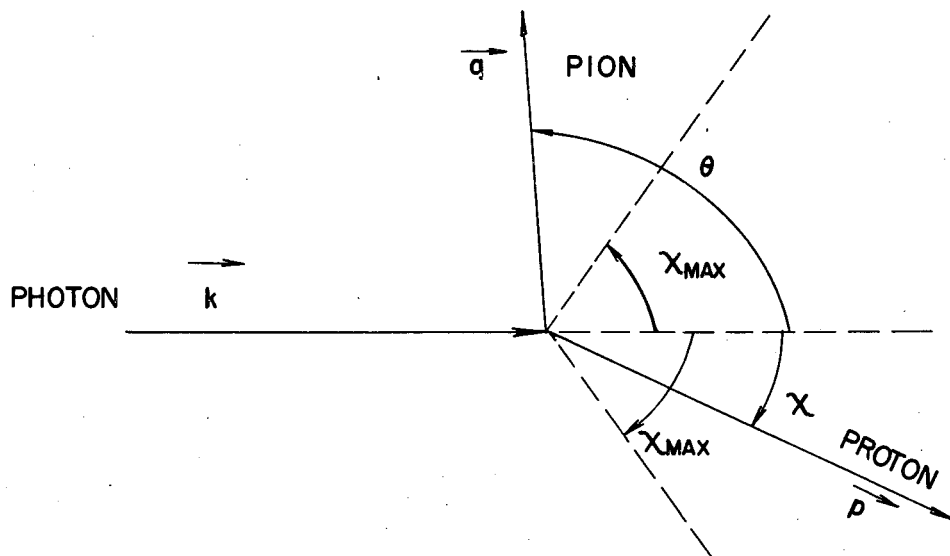


Fig. 4

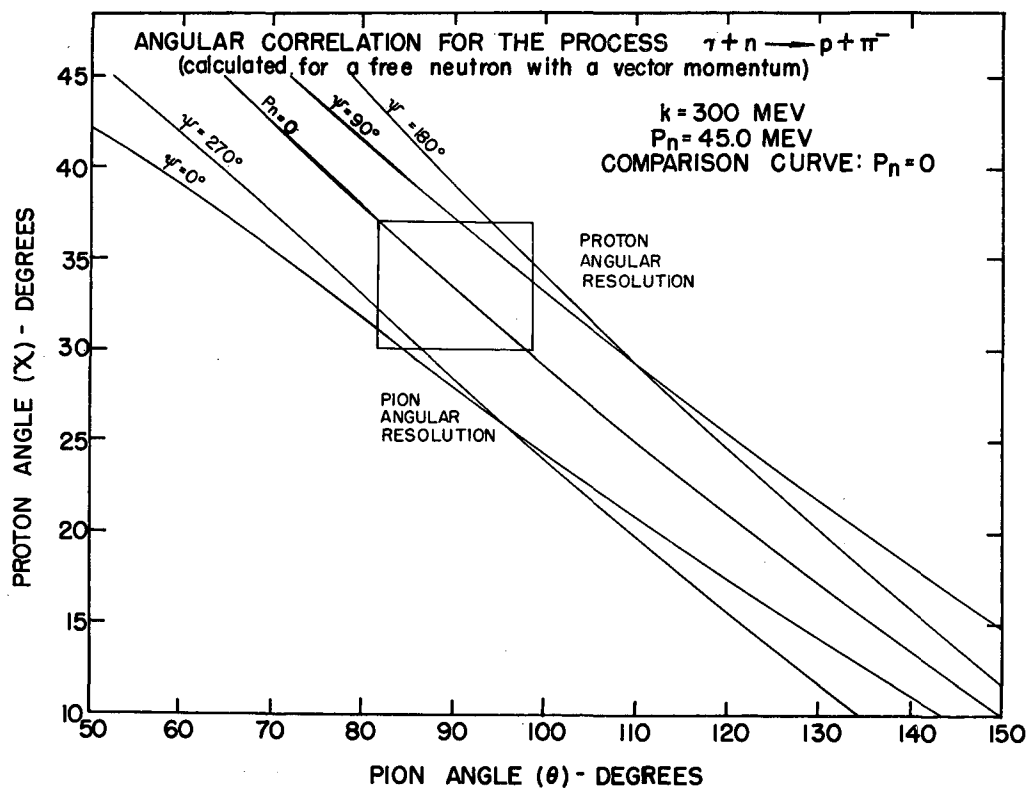


LABORATORY PION ANGLE θ IS CHOSEN GREATER THAN
MAXIMUM THEORETICAL PROTON ANGLE χ_{MAX}

VECTOR MOMENTUM DIAGRAM

MU 2928

Fig. 5



MU 2936

Fig. 6

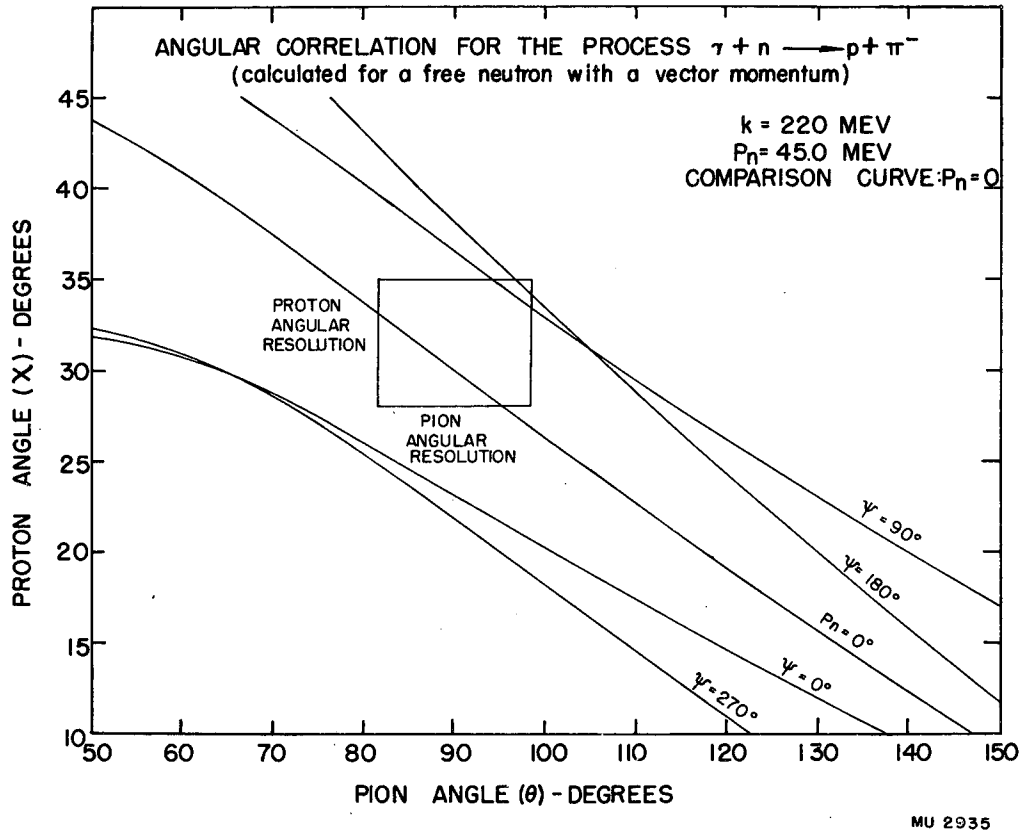
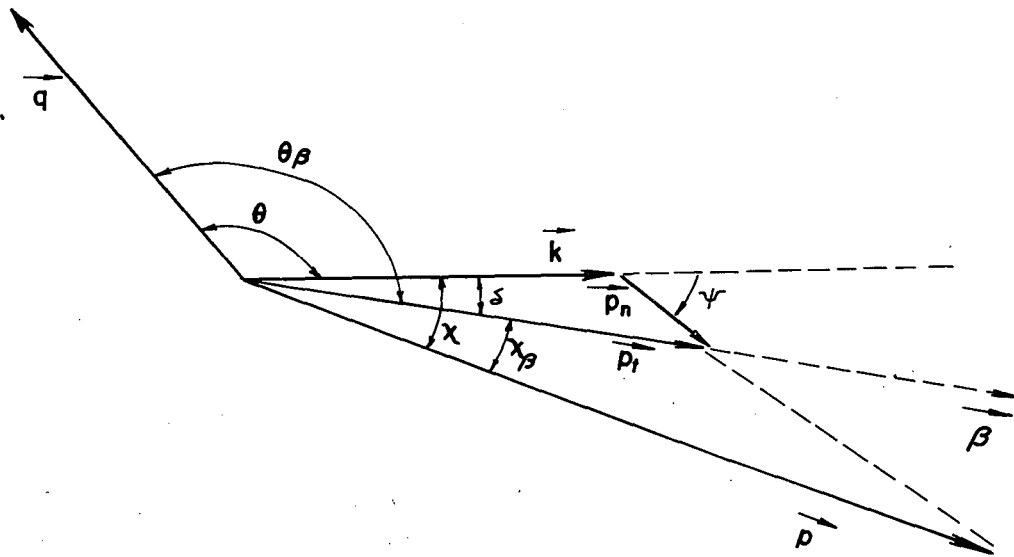


Fig. 7



LABORATORY VECTOR MOMENTUM DIAGRAM FOR THE PHOTOPION PRODUCTION FROM A FREE NEUTRON WITH A VECTOR MOMENTUM

MU 2929

Fig. 8

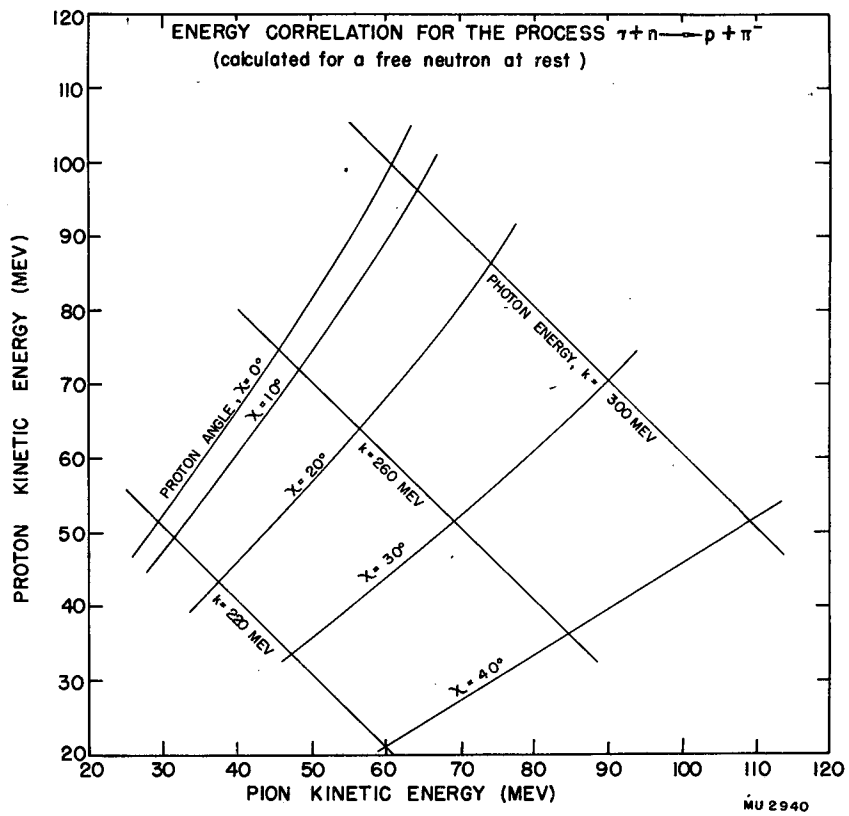
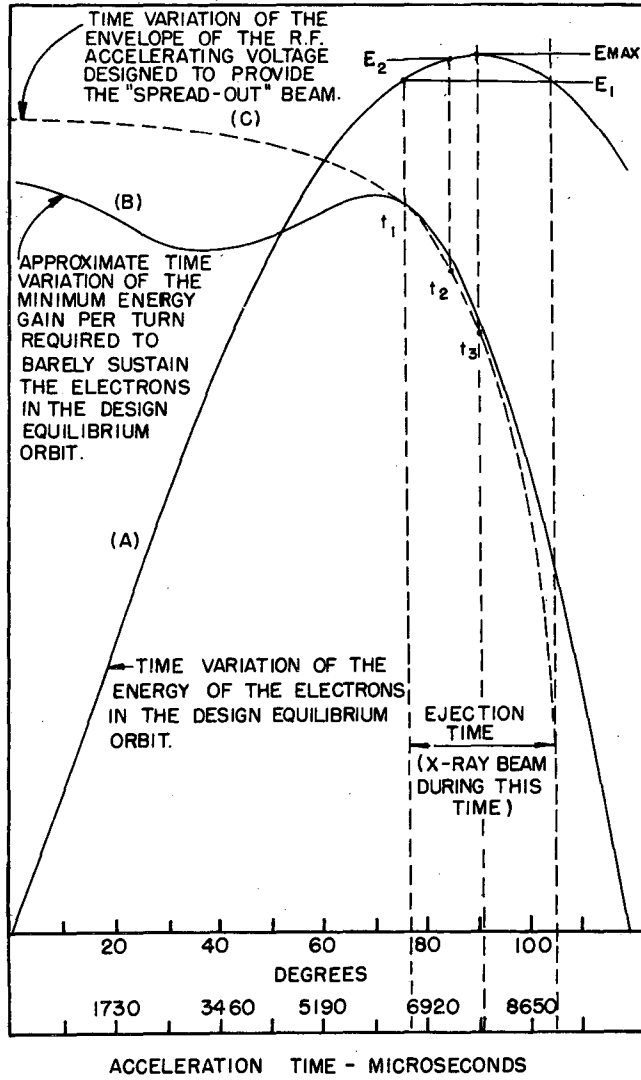


Fig. 9



MU 2951

Fig. 10

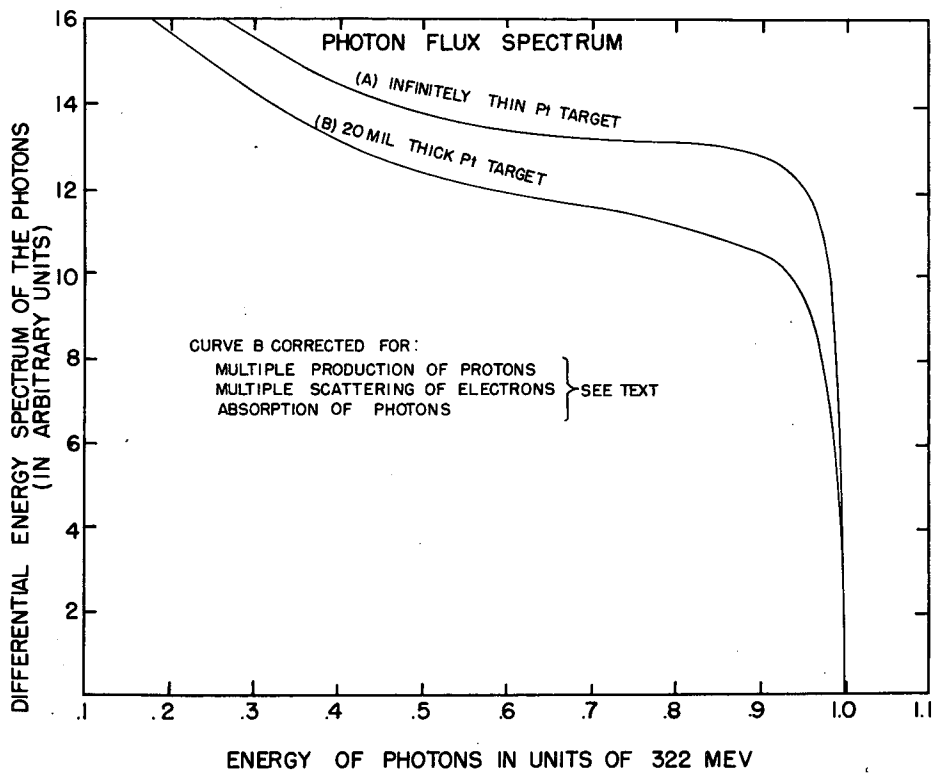
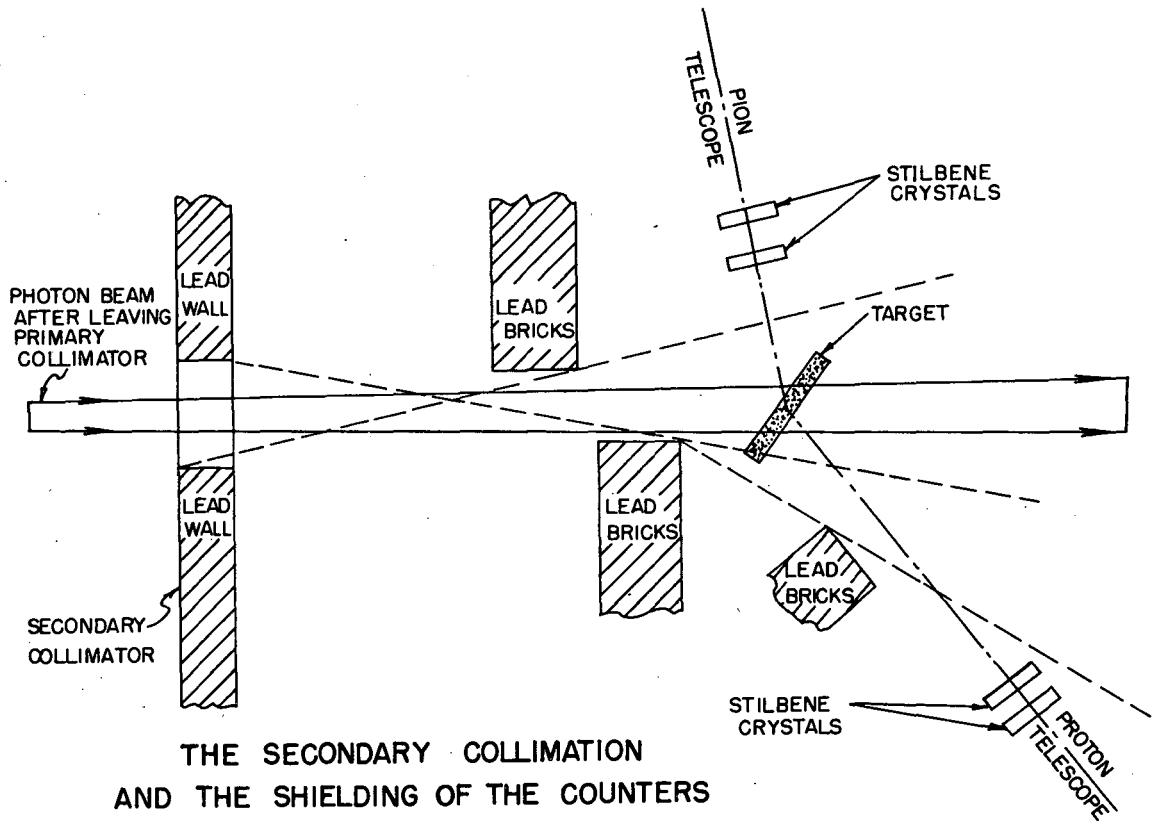


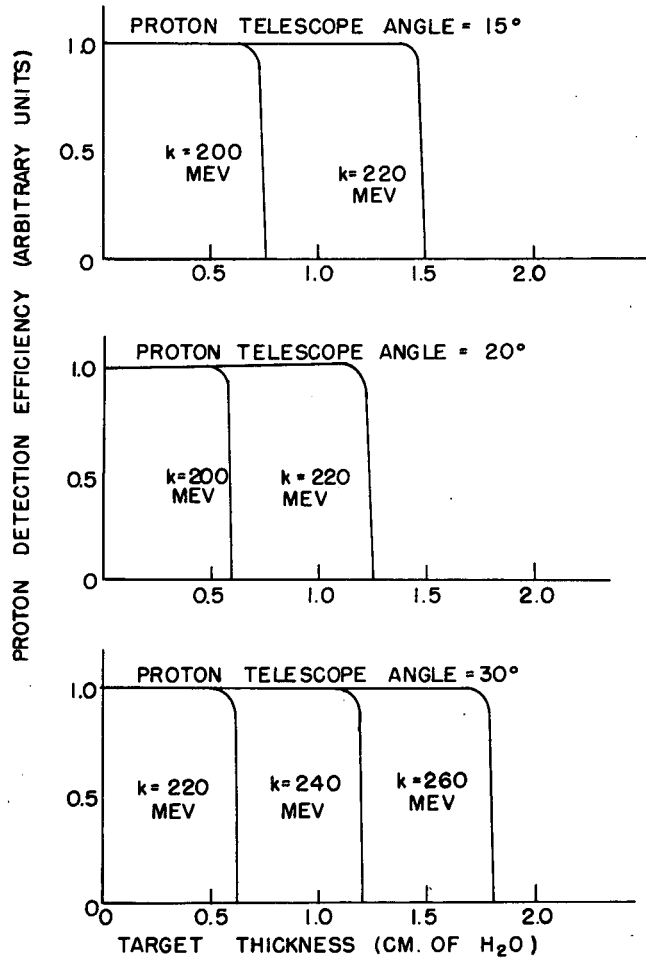
Fig. 11



MII 2930

Fig. 12

PROTON DETECTION EFFICIENCY vs. TARGET THICKNESS



MU 2924

Fig. 13

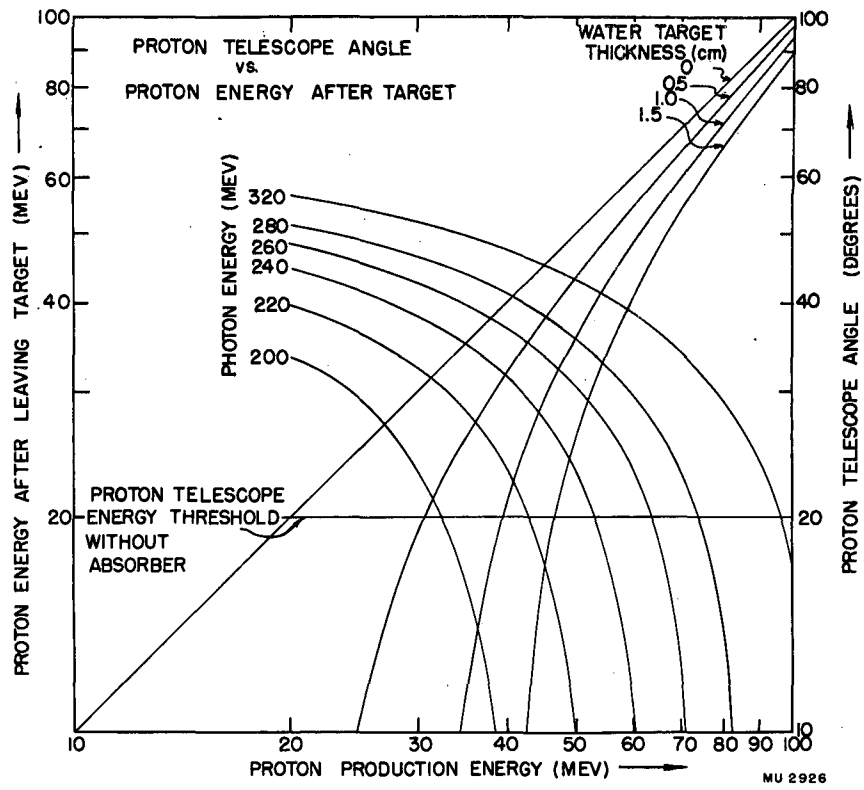


Fig. 14

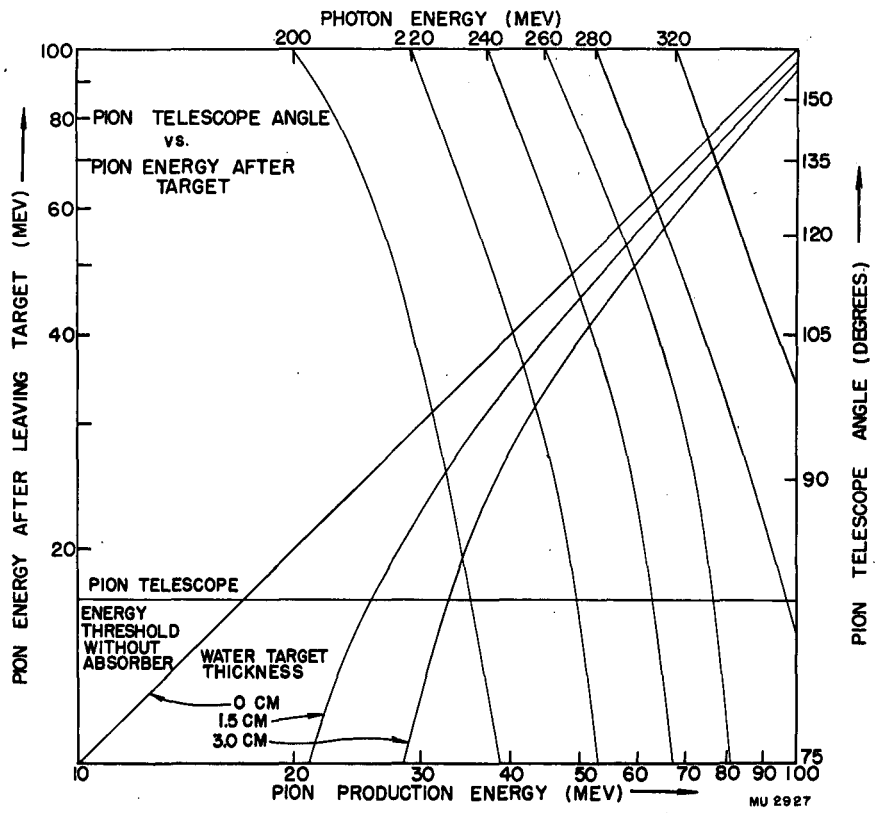
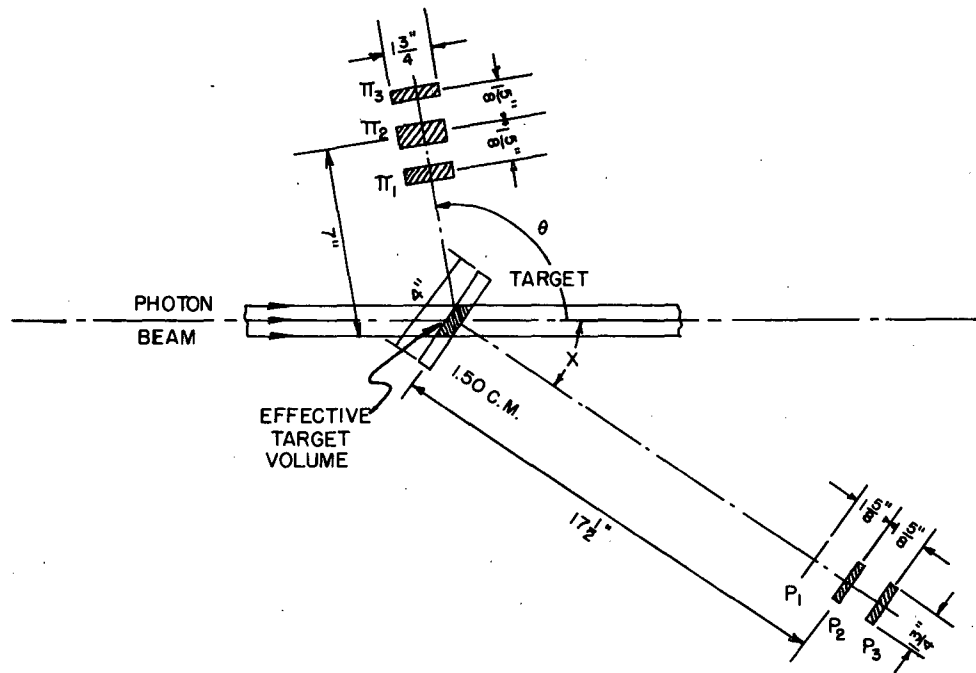


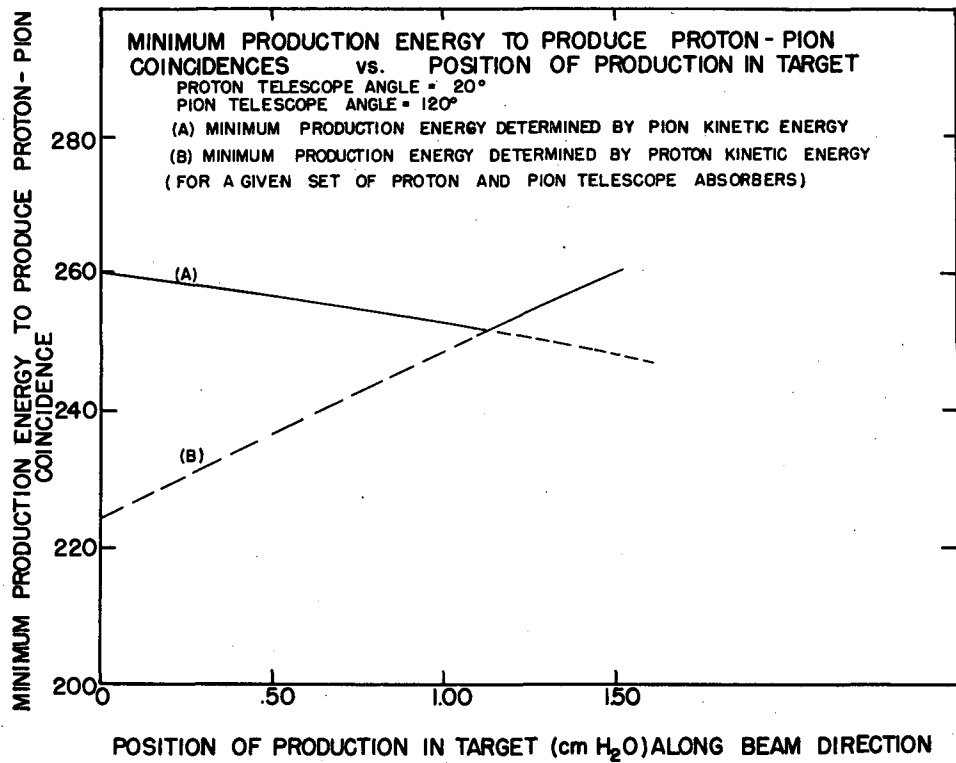
Fig. 15

THE GEOMETRY OF THE SCINTILLATION COUNTER TELESCOPES



MU 2931

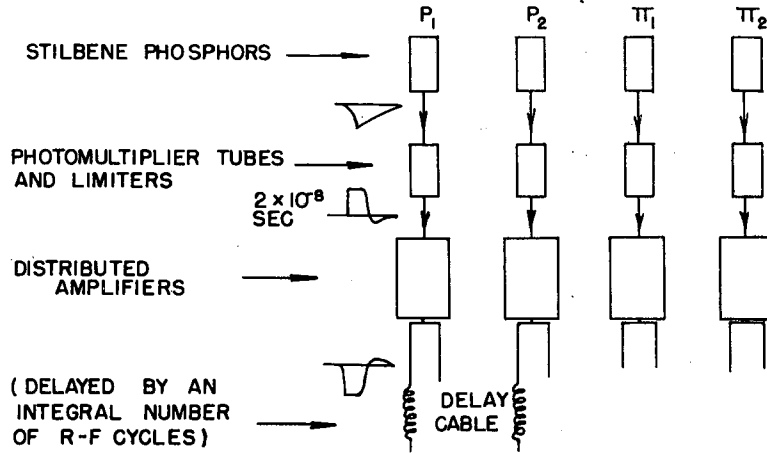
Fig. 16



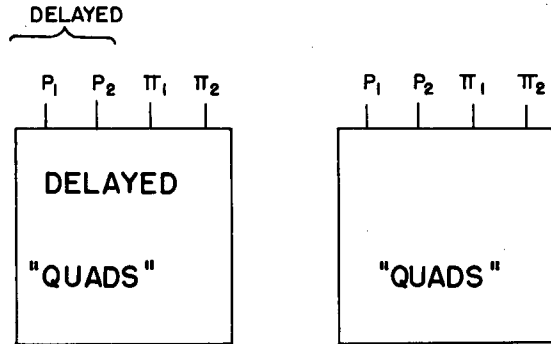
MU 2925

Fig. 17

BLOCK DIAGRAM OF ELECTRONICS-FIRST ARRANGEMENT

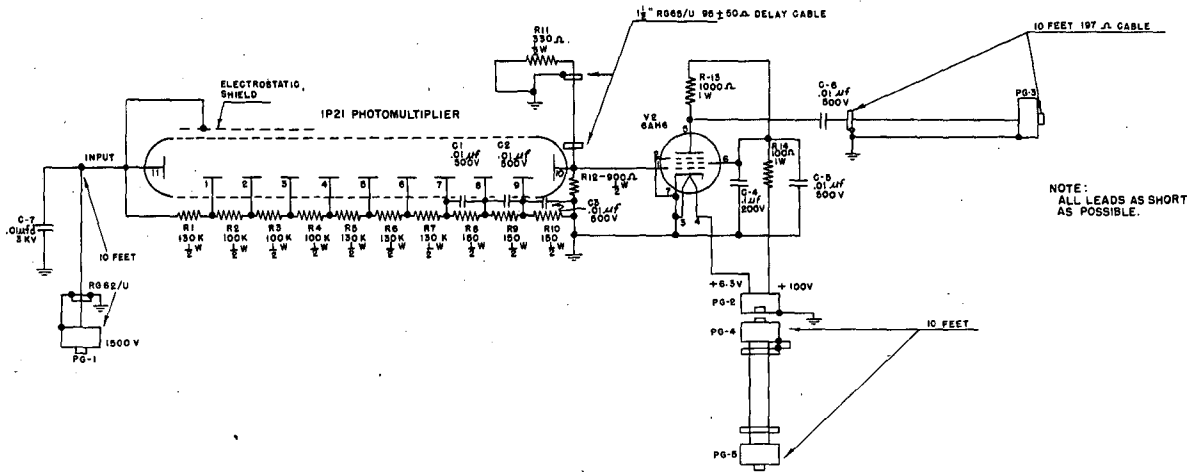


TIME RESOLUTION $\sim 2 \times 10^{-8}$ SEC.



MU 2933

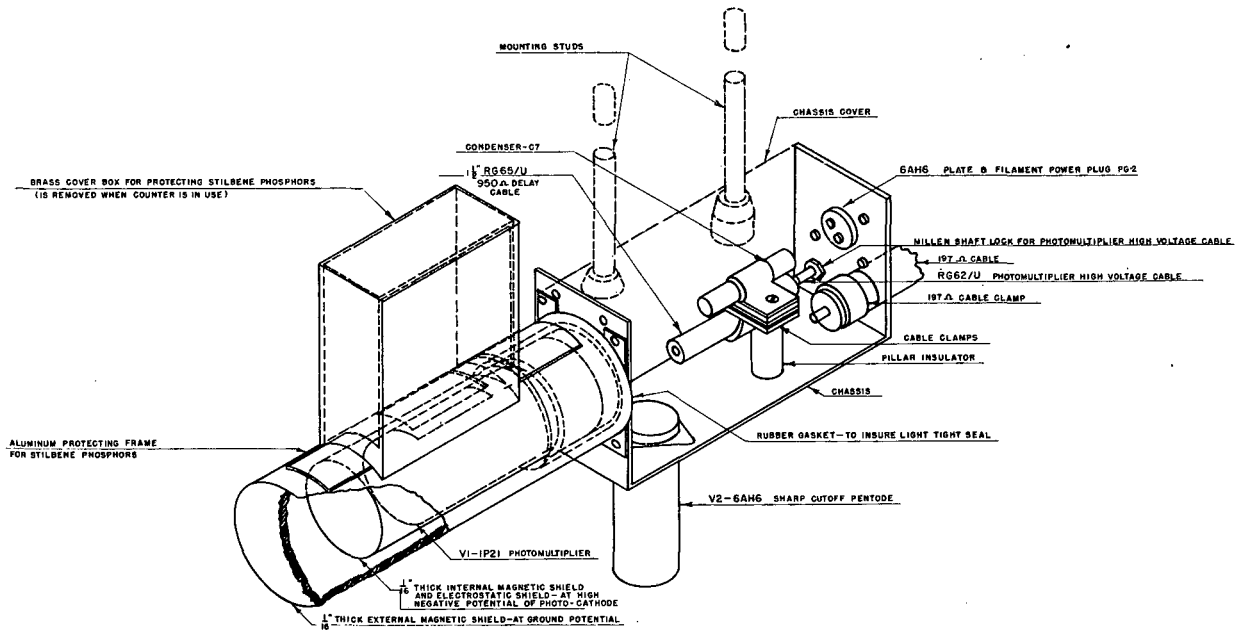
Fig. 18



PHOTOMULTIPLIER AND LIMITER

MU3032

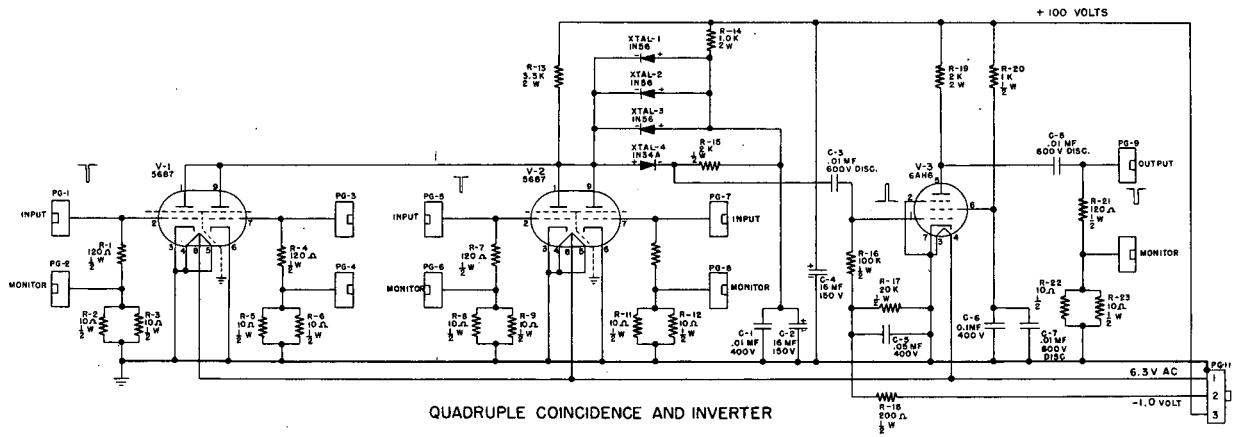
Fig. 20



PHOTOMULTIPLIER AND LIMITER CIRCUIT ASSEMBLY

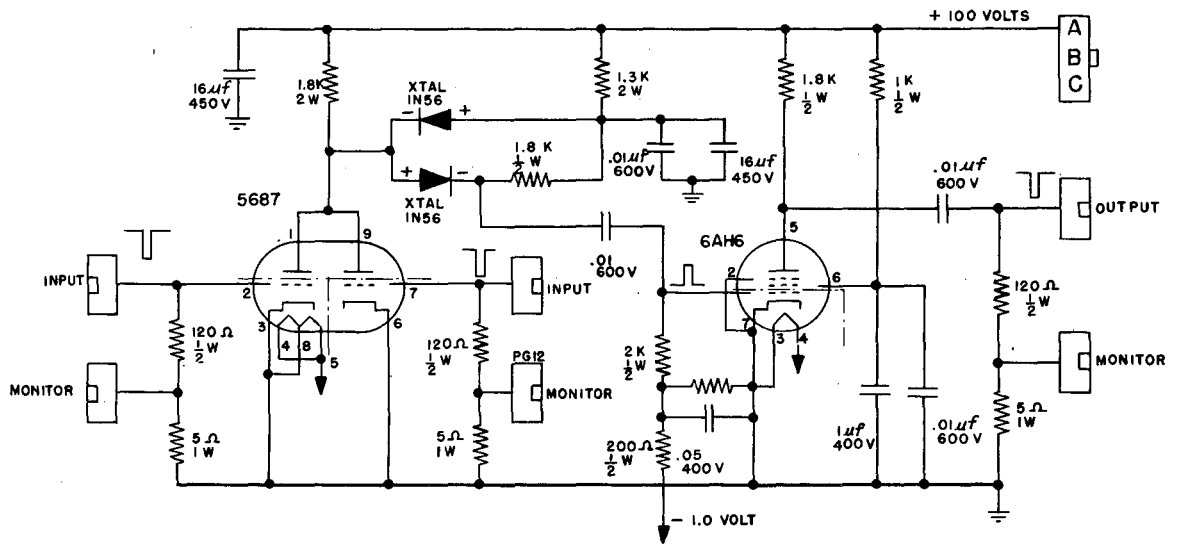
MU3028

Fig. 21



MU3031

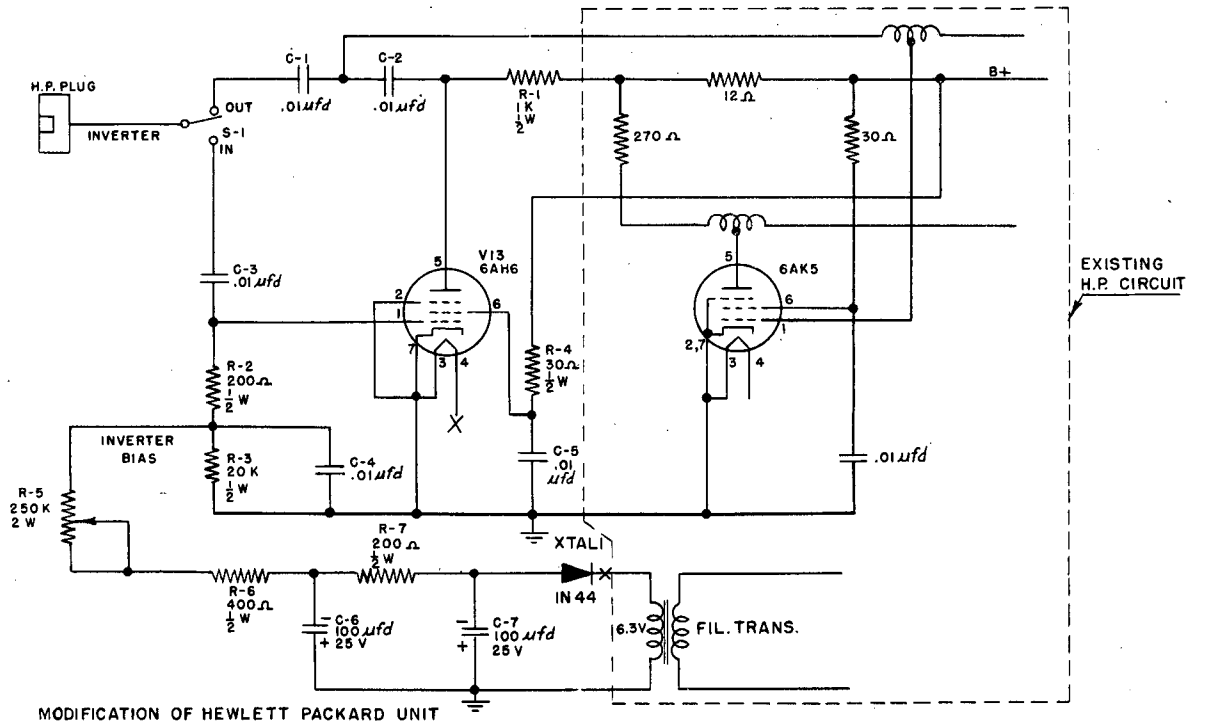
Fig. 22



DOUBLE COINCIDENCE AND INVERTER

MU3029

Fig. 23



MODIFICATION OF HEWLETT PACKARD UNIT

HEWLETT PACKARD WIDE BAND AMP MODEL 460 A
PHASE INVERTER

MU3030

Fig. 24

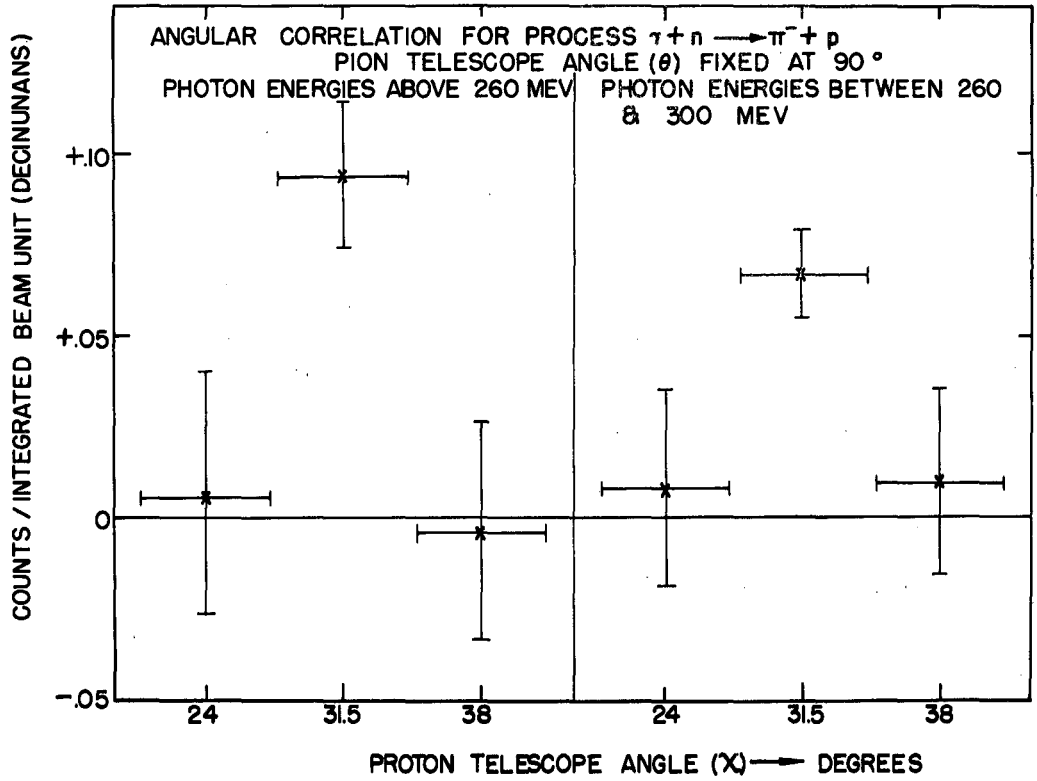


Fig. 25

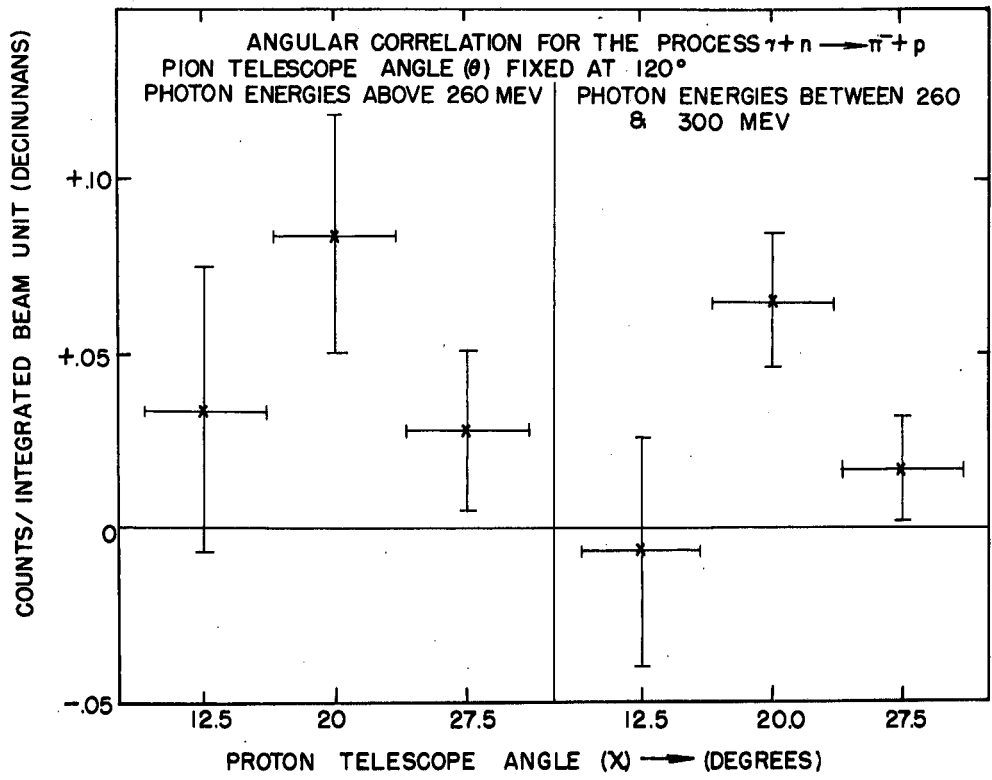
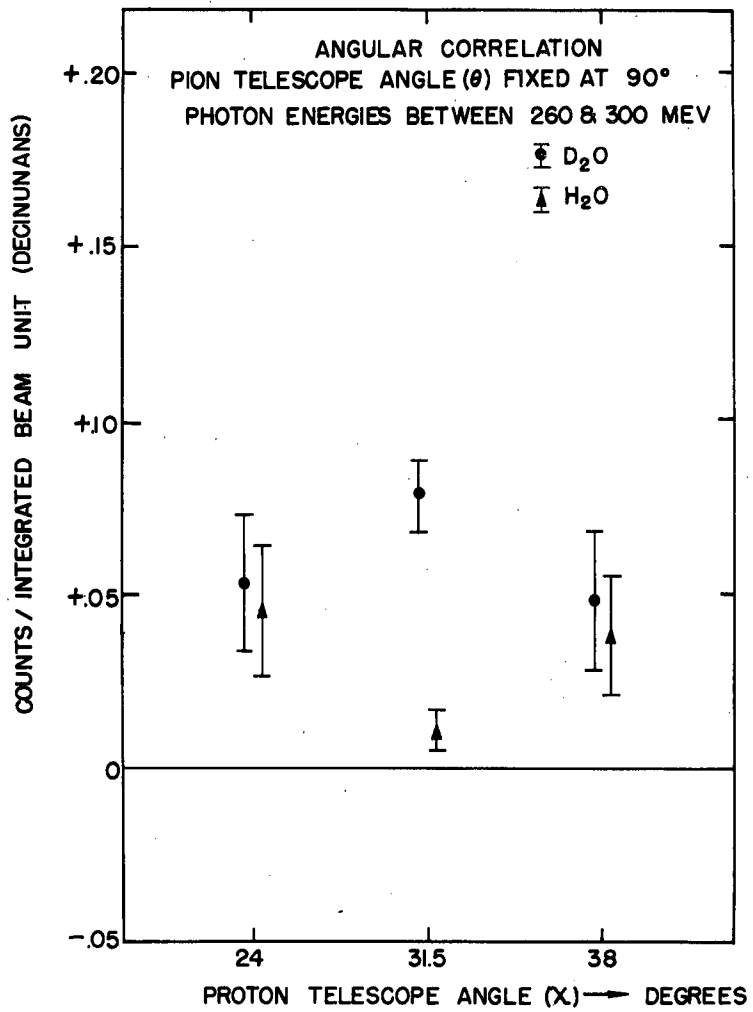
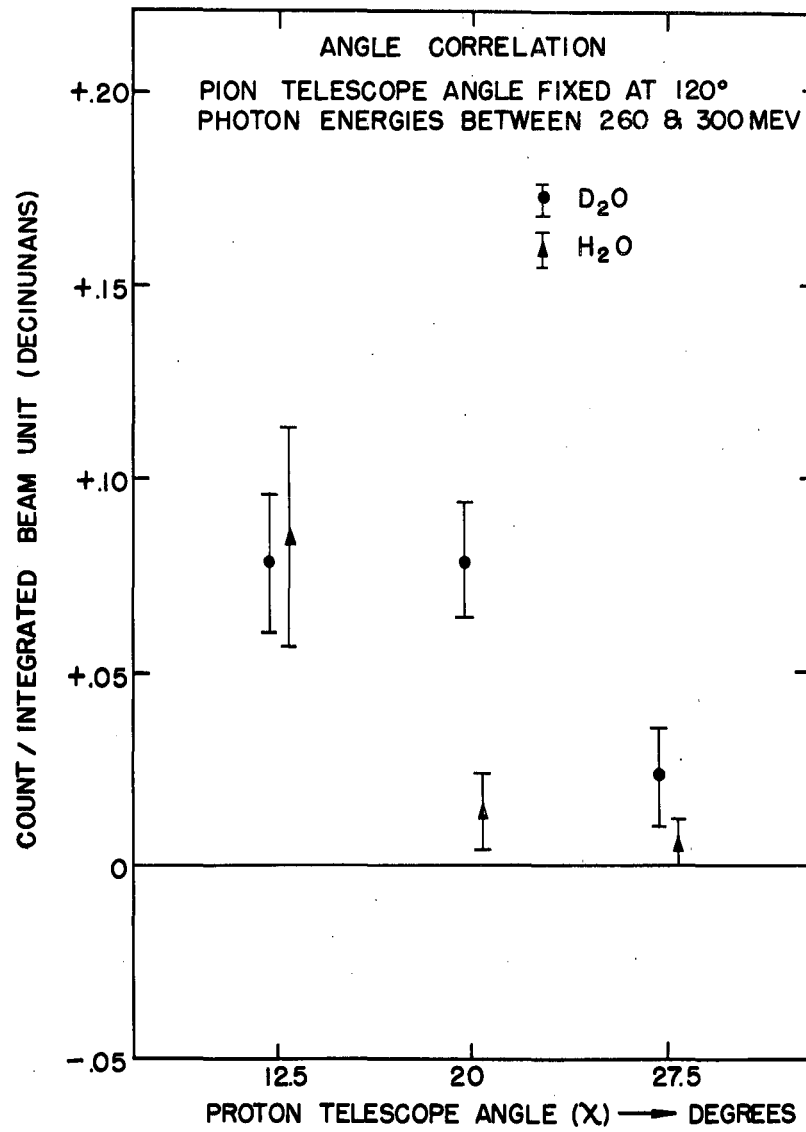


Fig. 26



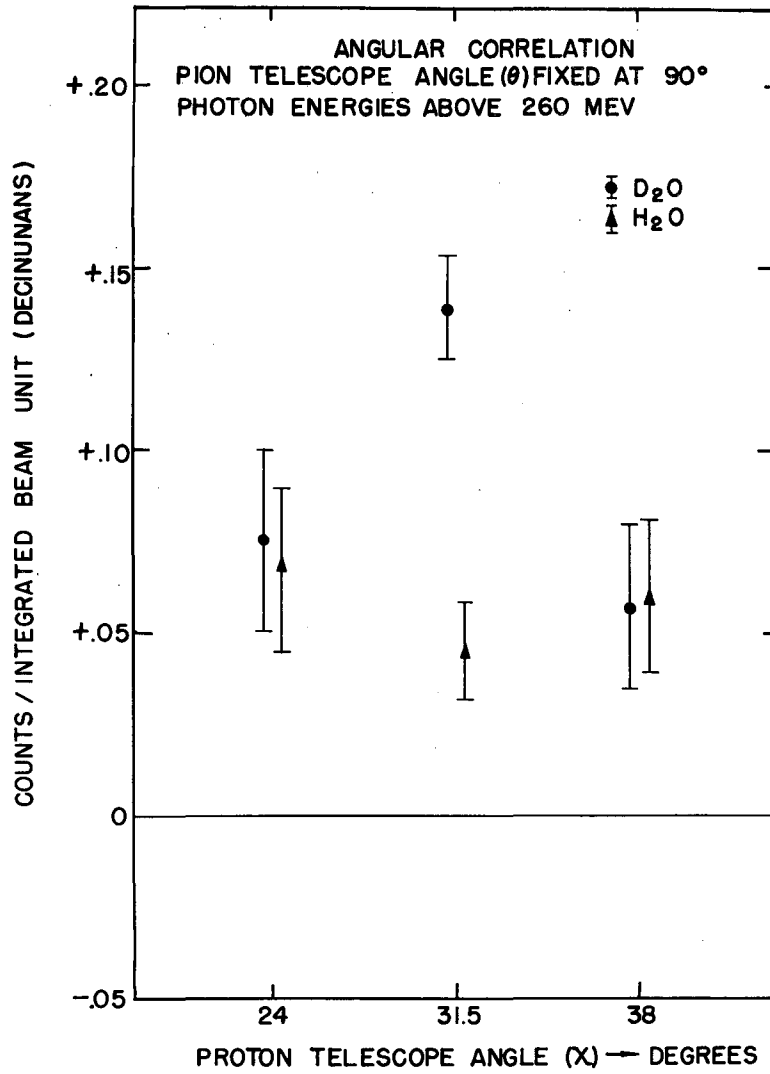
MU 2944

Fig. 27



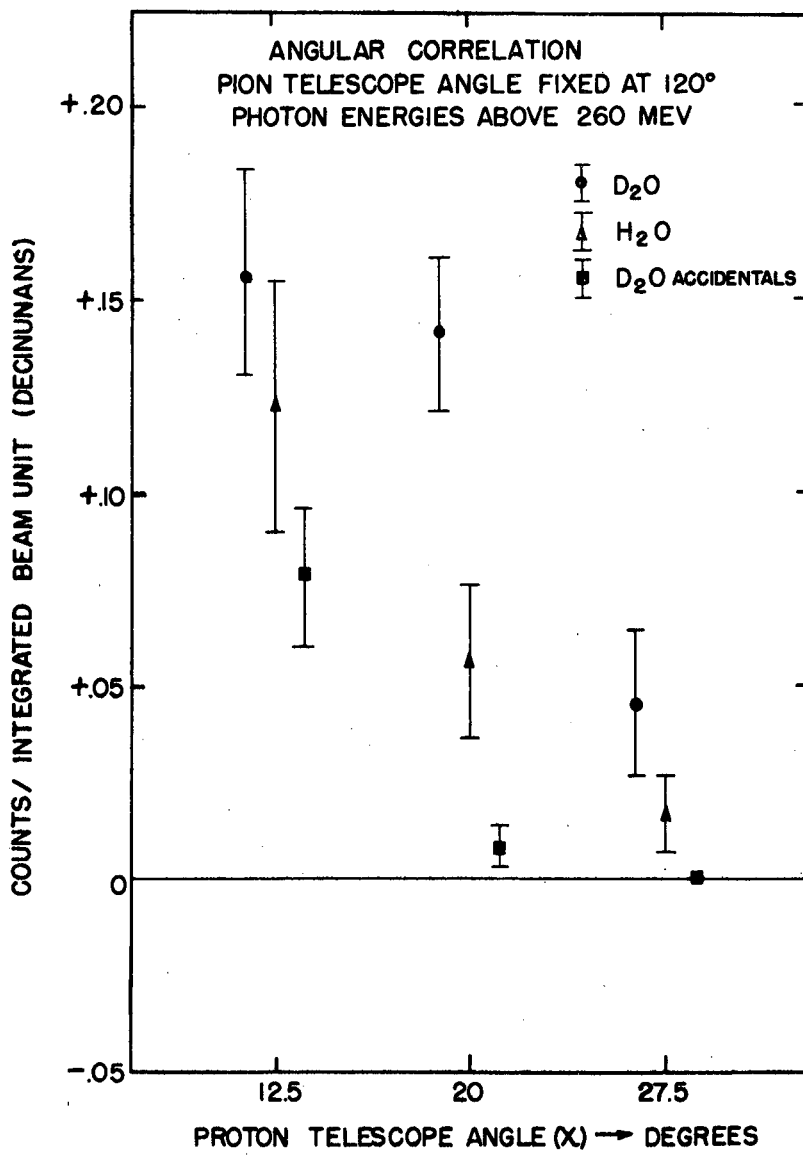
MU 2946

Fig. 28



MU 2943

Fig. 29



MU 2947

Fig. 30